Piezoelectric Nanogenerators Derived Self-Powered Sensors for Multifunctional Applications and Artificial Intelligence

Xiaole Cao, Yao Xiong, Jia Sun, Xiaoxiao Zhu,* Qijun Sun,* and Zhong Lin Wang*

With the arrival of the Internet of Things (IoTs) era, there is a growing requirement for systems with many sensor nodes in a variety of fields of applications. The demands for wireless, sustainable and independent operation are becoming more and more important for large-scale sensor networks and systems. For these purposes, a self-powered sensory system that can utilize the self-harvested energy from its surroundings to drive the sensors and directly sense external stimuli has attracted great attention. The invention and rapid development of piezoelectric generators (PENGs), which take Maxwell's displacement current as the driving force, has been pushing forward research on self-powered active mechanical sensors, electronic skins, and human-robotic interaction. Here, this review starts with a brief introduction of piezoelectric materials, fabrication, and performance improvement. Then, the energy harvesters used for self-power systems based on recent progress are reviewed. After that, PENGs applications toward recent self-powered active sensors are divided into four aspects and highlighted, respectively. Moreover, some challenges and future directions for the self-powered multifunctional sensors are put forward. It is believed that through the continuous investigations into PENG-based self-powered active sensors, they will soon be used in touch screens, electronic skins, health care, environmental monitoring, and intelligence systems.

1. Introduction

With the increasingly serious problems of the energy crisis and environmental pollution, it is necessary to develop and utilize clean renewable energy to meet the growing demand of human beings and realize the sustainable development of society. Various clean and renewable energy sources with sustainability and environmental friendliness, such as solar energy, water energy, wind energy, kinetic energy, and bioenergy are widely developed as substitutable energy sources to traditional fossil fuels. However, these energy sources are greatly affected by environmental factors; in addition, the power supply reliability is low and the cost is high. Mechanical energy is an energy form that widely exists in the environment but is usually wasted in daily life. Examples are vibrations, human motions, fluidic flows from wind and water, etc. It is renewable, clean and sustainable. Since 2006, the discovery of piezoelectric nanogenerators (PENGs) based on 1D zinc oxide nanowires (ZnO NWs) has demonstrated the potential to effectively transform mechanical energy into electrical energy.[1] After that, it has attracted great attention from researchers and achieved rapid development in mechanical energy harvesting.

Nowadays, owing to the rapid development of science and technology, portable mobile communication devices are mightily facilitating human life. The mobile electronic devices highly rely on the external power source while the restricted capacity of energy storage limits their

X. Cao, Y. Xiong, Prof. Q. Sun, Prof. Z. L. Wang
Beijing Institute of Nanoenergy and Nanosystems
Chinese Academy of Sciences
Beijing 101400, P. R. China
E-mail: sunqijun@binn.cas.cn; zhong.wang@mse.gatech.edu

X. Cao, Y. Xiong, Prof. Q. Sun, Prof. Z. L. Wang
School of Nanoscience and Technology
University of Chinese Academy of Sciences
Beijing 100049, P. R. China

Prof. J. Sun
School of Physics and Electronics
Central South University
Changsha 410083, P. R. China

Prof. X. Zhu
Beijing Institute of Fashion Technology
Beijing 100029, P. R. China
E-mail: 20180010@bift.edu.cn

Prof. Q. Sun
Center on Nanoenergy Research
School of Physical Science and Technology
Guangxi University
Nanning 530004, P. R. China

Prof. Z. L. Wang
School of Materials Science and Engineering
Georgia Institute of Technology
Atlanta, GA 30332, USA

2102983 (1 of 31)

**ADVANCED
SCIENCE NEWS**
www.advancedsciencenews.com

**ADVANCED
FUNCTIONAL
MATERIALS**
www.afm-journal.de

operation life. The concept of self-powering is an attractive solution to continuous power supply for the portable communication devices. The PENGs, which can readily convert mechanical energy from surroundings into electrical energy, provide a potential method as a self-powered source. Compared with conventional piezoelectric energy harvesters, PENGs can convert mechanical energy into electrical energy in the nanometer range. Larger specific surface area in the active piezoelectric materials with micro–nanostructures lead to better output performance in PENGs. Besides, PENG also has the advantages of strong universality, small size, high output performance, easy processing, excellent flexibility and adaptability, etc. These characteristics make PENG a promising candidate for low-energy power sources in such fields as microelectronic systems, medical implant devices, wearable electronic devices, etc. These characteristics make PENGs a promising candidate for low-energy power sources in such fields as microelectronic systems, medical implant devices, wearable electronic devices, etc.[2–4]

Moreover, the rise of the Internet of Things (IoTs) relies on the construction of large-scale sensor networks and systems. In the context of current sensory technology, most sensors require electrical power for regular operations. Therefore, it is particularly important to realize the self-powered operation of sensor nodes in sensor networks, wireless communication, and signals transmissions. In addition to PENGs' excellent function as a sustainable power supply for electronic devices, the electrical signal generated by them can also be used to directly sense the applied mechanical action without an external power supply. PENGs can also act as active sensors and extend for different types of mechanical motions. In the past decades, researchers have been devoted to developing nanogenerators with high output, conversion efficiency, and sensitivity from the perspective of materials and structures, and using them as flexible/wearable power supplies of self-powered systems in various multifunctional sensors.

In recent years, some outstanding review papers have been published, concerning on the application of PENGs in different and specific research areas. For instance, Zhao et al. summarized flexible nanogenerators for wearable electronic applications based on piezoelectric materials, which lights on exploration of new materials, devices, and technologies on piezoelectricity.[5] Hu et al. introduced some strategies to achieve high performance piezoelectric nanogenerators from the aspects of piezoelectric matrix, surface morphology engineering, physical/chemical doping, etc.[6] They also predicted the future prospects and directions of PENGs. Hu and Wang forced on piezoelectric nanogenerators as a sustainable power source in self-powered systems and active sensors.[4] And Liu et al. systematically presented the development of high-performance tactile sensors applied in intelligent systems.[7] Here, this paper delivers a comprehensive review of the recent development of PENGs, covering the typical piezoelectric materials, the fabrication process, strategies for the enhancement of piezoelectric performance, and multifunctional application of the piezoelectric nanogenerators. In addition, the applications of PENGs are mainly divided into two aspects. The first part is the intrinsic energy-harvesting applications of PENGs based on human activities and the surrounding environment. The other significant application of PENGs is to work as self-powered

sensors for measurement of human body signals, monitoring of environmental conditions, biomedical applications, and artificial intelligence (**Figure 1**). Finally, future directions of the self-powered multifunctional sensors are discussed. This review mainly includes the research progress in the recent five years.

2. Materials, Fabrication, and Performance Enhancement

2.1. Piezoelectric Materials

Natural quartz is the first discovered piezoelectric material by French physicists Jacques and Pierre Curie in 1880. The destruction of central symmetry in the crystal structure caused by external mechanical stimulation can induce piezoelectric potential in piezoelectric materials, which is pivotal to understand the structure and performance and to link material and function.[8] Afterward, piezoelectric materials and related piezoelectricity have attracted extensive attention from modern science and technology worldwide. Meanwhile, many other natural piezoelectric materials have been found and a lot of artificial piezoelectric materials with excellent performance have been synthesized to meet various application requirements during the last 140 years. As biopiezoelectric materials potentially offer a simple and environmentally friendly approach to energy generation, smart sensing, and artificial intelligence, we specially classify the piezoelectric materials into three types in this review: common inorganic and polymer materials, and biomaterials (to be emphasized). This part mainly reviews the recent research progress in piezoelectric materials.

2.1.1. Inorganic Piezoelectric Materials

PENG was first proposed in 2006[1] and has been rapidly developed in recent years. For the active materials, inorganic piezoelectric materials have been widely used in the manufacture of PENGs for energy harvesting or working as self-powered sensors.[5] Inorganic piezoelectric materials are traditionally divided into piezoelectric crystals and piezoelectric ceramics.[9,10] Piezoelectric crystals generally refer to piezoelectric single crystals, which are crystals grown in a long-range order in a lattice of crystal space. This crystal structure has no center of symmetry, resulting in natural piezoelectricity. Examples can be found from crystal (quartz) and ZnO NWs. Zinc oxide, a well-known dielectric, transparent, piezoelectric and wide band-gap material, has been reported for a large range of applications such as the piezoelectric transducer, gas sensor, and energy harvesting with nanogenerators.[11–14] **Figure 2**a shows the crystal structure of wurtzite ZnO and the induced piezoelectric potential distributions under external tensile/compressive strains. In the original state, the tetrahedrally coordinated Zn^{2+} and O^{2-} are stacked layer by layer along the c-axis and the charge centers of cations and anions coincide with each other. When an external tensile force is uniformly acted on the nanowire surfaces, the charge centers of the cation and anion are separated and form an electric dipole to induce a piezoelectric potential.[15] When the ZnO NW is connected to an external load, the piezoelectric
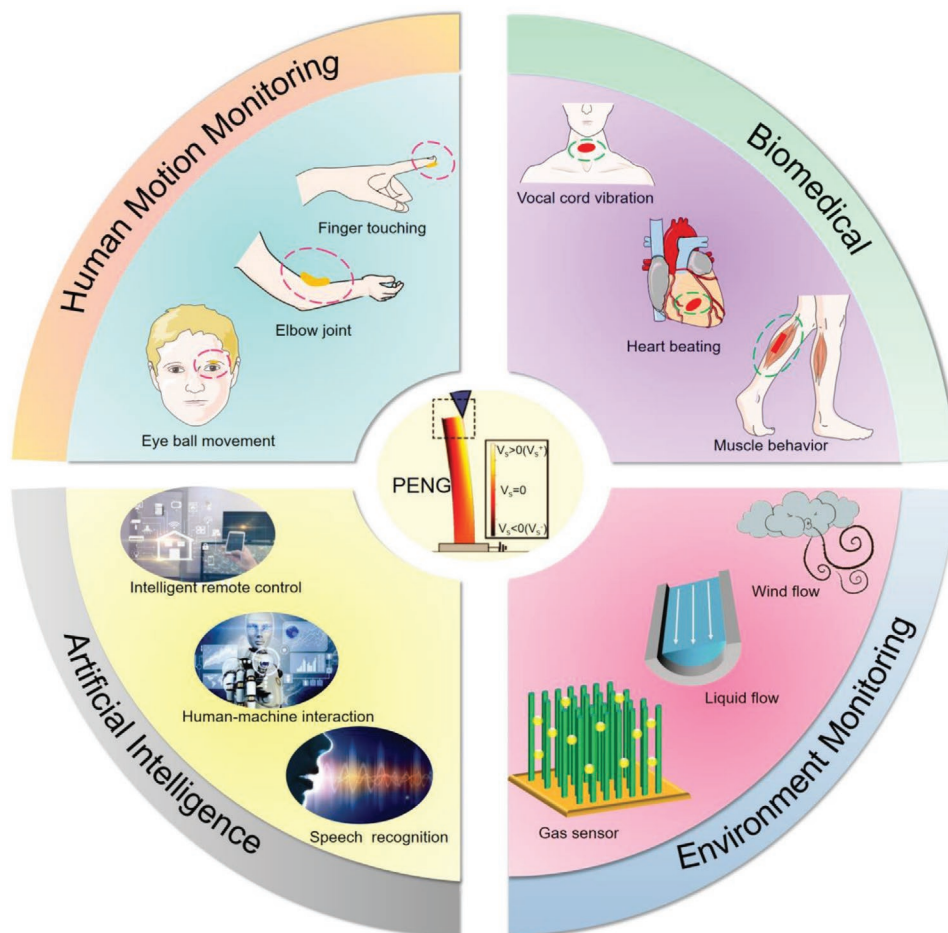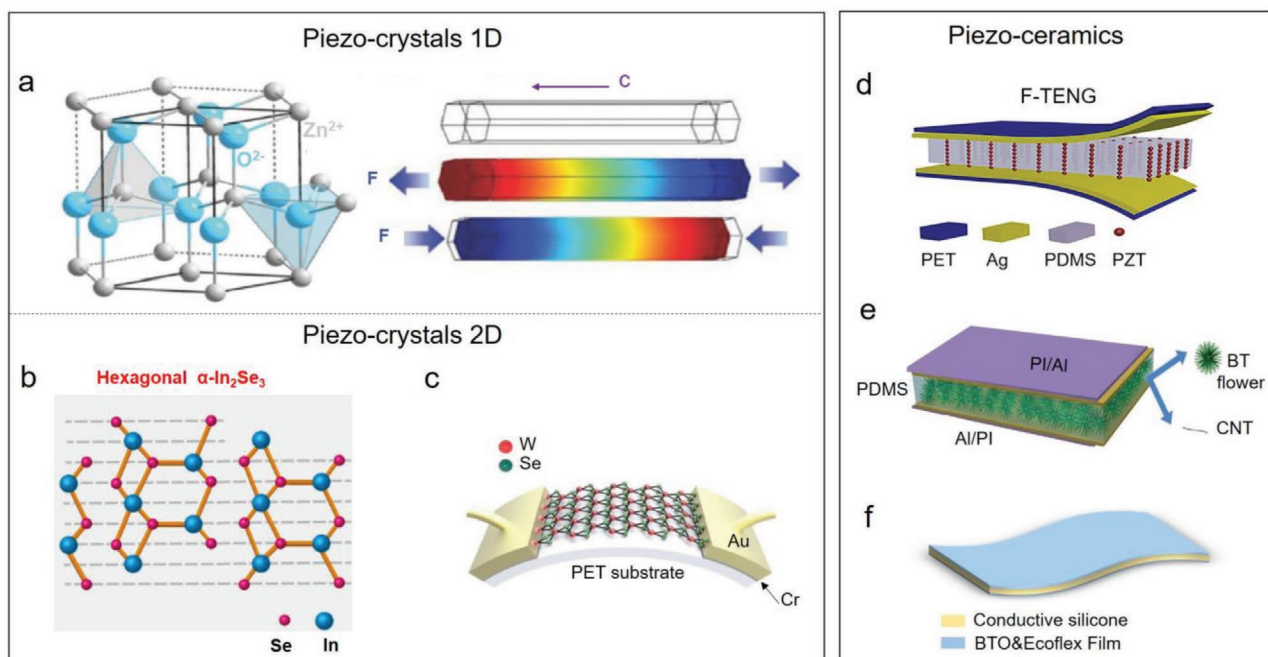
**ADVANCED
SCIENCE NEWS**
www.advancedsciencenews.com

**ADVANCED
FUNCTIONAL
MATERIALS**
www.afm-journal.de

Figure 1. Application of active self-powered sensors based on piezoelectric nanogenerator.[1]

potential will drive electrons to flow through the external load until the electrons partially shield the piezoelectric potential to reach a new equilibrium state. Thus, the conversion from mechanical energy to electrical energy is realized. ZnO is a promising material choice for PENGs due to its relatively large piezoelectric coefficient (d_{33}), abundance, environment-friendly nature, and biocompatibility. Although ZnO exhibits low dielectric constant (εr) and moderate piezoelectric strain constant (E), it possesses higher piezoelectric voltage constant and can be readily fabricated into different nanostructures for flexible PENGs.[16–18] In recent years, to improve the output performance and develop diversified applications, researchers have also developed various structures of ZnO such as nanowires, nanorods, nanosheets, and nanobows to construct piezoelectric nanogenerators.[19–21]

2D single crystal materials as high-performance piezoelectric materials have also attracted great attentions.[22–27] Molybdenum sulfide (MoS_2) is predicted to have a strong piezoelectric effect, which disappears in the bulk owing to the opposite orientations of adjacent atomic layers.[28] Layered materials, such as hexagonal boron nitride (h-BN), graphite, and many transition-metal dichalcogenides (TMDCs) exhibit different symmetry after being thinned down to a single atomic layer.[29,30] Wu et al. conducted the first experimental

study of the piezoelectric properties of 2D MoS_2.[25] The results showed that the periodic stretching and releasing of the thin MoS_2 sheet with odd atomic layers induced oscillatory piezoelectric voltage and current output. Xue et al. experimentally researched the piezoelectricity of α-In_2Se_3 from monolayer to bulk material and developed a multilayer α-In_2Se_3-based PENG (Figure 2b).[31] Lu et al. reported a synthetic strategy for growing Janus monolayers of TMDCs that broke the out-of-plane structural symmetry by especially replacing the top-layer S with Se atoms based on monolayer MoS_2,[32] and they proved the existence of vertical dipoles. Lee et al. synthesized mono/bilayer tungsten diselenide (WSe_2) via chemical vapor deposition (CVD) and also proved its piezoelectricity.[33] Figure 2c shows the schematic of piezoelectric energy harvesters (PEHs) based on monolayer WSe_2, which demonstrates its potential for being used in mechanical sensors and serving as energy sources for wearable and body implantable devices.

In addition to the above-mentioned emerging nanostructured inorganic piezoelectric materials, traditional piezoelectric ceramics have also made great progress in the field of energy harvesters because of its high piezoelectric coefficient and good mechanical properties. **Table 1** compares the performance of different piezoelectric materials. Piezoelectric ceramics refer to piezoelectric polycrystals that are consisted

ADVANCED
SCIENCE NEWS
www.advancedsciencenews.com

ADVANCED
FUNCTIONAL
MATERIALS
www.afm-journal.de

Figure 2. a) Atomic model of the wurtzite-structured ZnO, 3D views, and numerical calculation of the piezoelectric potential distribution in a ZnO NW under axial strain. Reproduced with permission.[15] Copyright 2009, American Institute of Physics. b) The side view for atomistic arrangement structure models of α-In$_2$Se$_3$. Reproduced with permission.[31] Copyright 2018, American Chemical Society. c) Schematic of the PEH based on monolayer WSe$_2$. Reproduced with permission.[33] Copyright 2017, Wiley-VCH GmbH. d) Oriented particle structure of F-PENG. Reproduced with permission.[35] Copyright 2020, John Wiley & Sons Ltd. e) Schematic of the composition of BTFs-CNTs/PDMS composites and the structure of the corresponding energy harvester. Reproduced with permission.[37] Copyright 2020, Wiley-VCH GmbH. f) Schematic diagram of BPNG. Adapted with permission.[38] Copyright 2020, Elsevier B.V.

of many small crystals with random crystal orientations. They generally require a polarization process to enhance the piezoelectricity by aligning the dipoles with an external electric field. Typical piezoelectric ceramics include lead zirconate titanate piezoelectric ceramics (Pb[Zr$_x$Ti$_{1-x}$]O$_3$, $0 \leq x \leq 1$, PZT), barium titanate (BaTiO$_3$), etc.[10] Jin et al. synthesized vertically aligned PZT nanorod arrays on a preoxidized Ti substrate by a one-step hydrothermal method using surfactants.[34] PZT nanorods exhibit a high-voltage electrical response, with a d_{33} value of up to 1600 pm V^{-1}. Zhang et al. prepared flexible piezoelectric nanogenerators with necklace-like oriented structure by dielectrophoresis (DEP).[35] The oriented structure helped to enhance the stress and free charge transmission, which significantly improved the electrical output performance of the PENG. PENG prepared by doping 8% oriented PZT particles (Figure 2d) could achieve an open circuit voltage (V_{OC}) of 176 V and a short circuit current (I_{SC}) of 35 μA.

However, because lead is harmful to the human body and the environment, none-lead (Pb) piezoelectric materials have also been developed. Shin et al. used nanoimprint technology to form uniformly patterned piezoelectric BaTiO$_3$ (BTO) nanopillars on a sol-gel coated polyethylene terephthalate (PET).[36] UV treatment on the patterned sol–gel layer contributed to further improve the crystallinity of the sol–gel BTO layer. Based on this, the prepared PENG obtained a voltage of 10 V and a current density of 2 μA cm^{-2}. As shown in Figure 2e, Jian et al. reported the polydimethylsiloxane (PDMS) composites filled with hierarchical BaTiO$_3$ flowers (BTFs).[37] The BTF-based PENG obtained a V_{OC} of 260 V, an I_{SC} of 50 μA, and a power of 1728 μW, which showed significantly enhanced energy scavenging properties compared with that of polymer composites filled with BT nanoparticles (NPs). They analyzed the simulated electric potential and stress under 50 N pressure through finite element analysis on PENGs. The simulation results showed that the petals of BTFs had shown more effective stress while

Table 1. Performance comparison of piezoelectric materials.[39–44]

Piezoelectric materials	Zinc oxide	Quartz crystal	Barium titanate (BaTiO$_3$)	Lead zirconate titanate (PZT-4)	PVDF	P(VDF-TrFE)
Piezoelectric coefficient [pC N^{-1}]	12.7	$d_{11} = 2.31$ $d_{14} = 0.73$	$d_{15} = 260$ $d_{31} = -78$ $d_{33} = 190$	$d_{15} \approx 410$ $d_{31} = -100$ $d_{33} = 230$	$d_{33} = 18$	$d_{31} = 20$ $d_{33} = -21$
Dielectric constants (εr)	10.3	4.5	1200	1050	8.4	10
Elastic modulus (10^9 N m^{-2})	146	80	110	83.3	0.92	0.45

**ADVANCED
SCIENCE NEWS**

www.advancedsciencenews.com

**ADVANCED
FUNCTIONAL
MATERIALS**

www.afm-journal.de

the center of the petals had a relatively smaller stress. Different from BT nanowires, under external pressure, the stress of the composite material was mainly distributed on the petals of BTFs, which helped to greatly enhance the performances. For better application in flexible wearable scenarios, Yu et al. reported a skin-conformal PENG based on BTO/Ecoflex, which was prepared through the incorporation of BTO particles into an Ecoflex matrix (Figure 2f).[38] Owing to the innate excellent tensile properties of Ecoflex, ultralow thickness of the BTO/Ecoflex film, and optimized polarization, the fabricated PENG shows proper skin-conformability and high output performance.

2.1.2. Piezoelectric Polymer Materials

Kawai first discovered strong piezoelectricity in poly(vinylidene fluoride) (PVDF) in 1969.[45] Compared with inorganic piezoelectric materials, piezoelectric polymers such as PVDF and its copolymer poly(vinylidenefluoride-co-tri-fluoroethylene) (P(VDF-TrFE)) are excellent in natural flexibility, light weight, easy-to-process feature, adequate mechanical strength, and long-term stability under a high electric field.[46–49] Up to now, five semicrystalline polymorphs of PVDF have been identified and labeled as α, β, γ, δ, and ε, respectively.[50] However, only β-phase PVDF has been proven to have strong piezoelectricity. The molecular model of β-phase PVDF shown in **Figure 3**a belongs to the orthorhombic system,[51] the molecular chain exhibits planar zigzag. The $-CF_2$ dipoles face the

same direction, and the molecular chains are arranged parallel to each other in the c-axis direction, which are preferential for the aligned dipoles to be enhanced and lead to an inner piezoelectric potential to generate piezoelectric charges on the polarization surface of the material. Accordingly, β-phase PVDF commonly has the largest spontaneous polarization properties ($P_s = 130$ mC m^{-2}). Over years, researchers have made many attempts in energy harvesting based on piezoelectric polymer materials.[52–55]

Pi et al. reported a flexible PENG with the P(VDF-TrFE) thin film as a functional layer.[56] This device achieved a V_{OC} of about 7 V, an I_{SC} of 58 nA, and a current density of 0.56 μA cm^{-2}. Ko et al. synthesized poly(2-butyl-2,3-dihydrothieno[3,4-b][1,4] dioxine:dodecyl sulfate (PEDOT-C$_x$:DS) by oxidative polymerization and used it as an electrode of the PVDF-based PENG with a sandwich structure (electrode/PVDF/electrode).[57] The composite conductive film had nanofiber-type 1D nanostructures after doping sodium dodecyl sulfate (SDS) in the PEDOT, which exhibited good conductivity (50 S cm^{-1}), aligned nanofibrillar network, highly ordered edge-on orientation and excellent dielectric constant (6.74). Based on the enhanced electrical conductivity and resultant hydrophobicity, the output performance of the fabricated PENG with doped PEDOT electrode is effectively improved by 53.7%. Liu et al. proposed an environmental-friendly and flexible PENG based on nanofiber mat composed of P(VDF-TrFE) and 0.5Ba(Zr$_{0.2}$Ti$_{0.8}$)O3-0.5(Ba$_{0.7}$Ca$_{0.3}$)TiO$_3$ (BZT-BCT).[58] The schematic of the nanogenerator is shown in Figure 3b. The device exhibited excellent output performance with an output voltage as
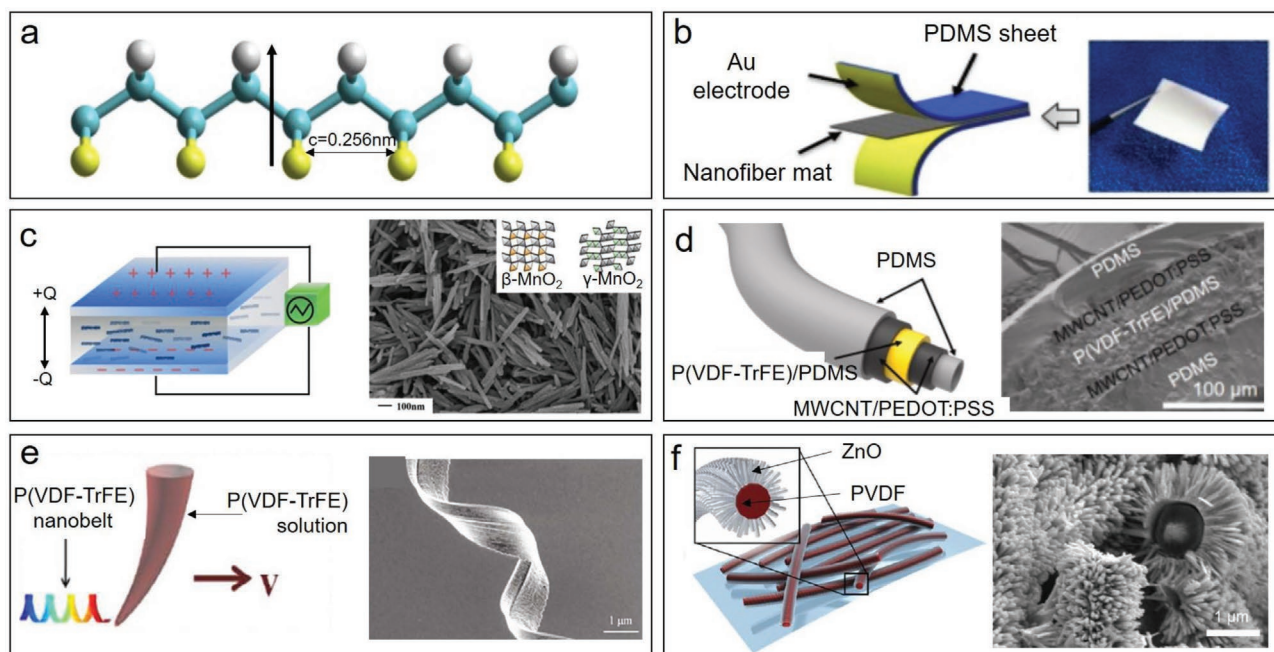
Figure 3. a) Structure of b-phase PVDF. Reproduced with permission.[51] Copyright 2008, Elsevier B.V. b) Schematic diagram of BZT-BCT/P(VDF-TrFE) nanogenerator and the picture of BZT-BCT/P(VDF-TrFE) nanofiber film. Reproduced with permission.[58] Copyright 2020, Elsevier B.V. c) The principle of the PENG based on the piezoelectric nanocomposites and SEM image of MnO$_2$ nanoparticles; inset is the schematic diagram of β-MnO$_2$ and γ-MnO$_2$. Reproduced with permission.[59] Copyright 2020, Elsevier Ltd. d) Schematic illustration of stretchable multifunctional (SMF) fiber and the SEM image of SMF fiber cross-section. Reproduced with permission.[60] Copyright 2018, Elsevier Ltd. e) The schematic of the fabrication of the P(VDF-TrFE) nanobelt by the direct-write technique and SEM image of P(VDF-TrFE) nanobelt. Reproduced with permission.[61] Copyright 2020, Wiley-VCH GmbH. f) The structure of core–shell PVDF/ZnO nanofibers and the cross-sectional SEM image of the PVDF/ZnO nanofiber. Reproduced with permission.[62] Copyright 2020, Elsevier Ltd.

ADVANCED
SCIENCE NEWS
www.advancedsciencenews.com

ADVANCED
FUNCTIONAL
MATERIALS
www.afm-journal.de

high as 13.01 V in the case of cyclic tapping under 6 N and at a frequency of 10 Hz. The nanogenerator was sensitive to microforce and delivered the output voltage in a good linear relationship within the load force; hence, it could be used as a sensitive self-powered sensor. Zhao et al. reported a flexible PENG based on a novel textured hybrid film consisting of PVDF and manganese dioxide (MnO_2) nanorods (Figure 3c).[59] Having a V_{OC} of 3.2 V with the hybrid films (with pure PVDF of only 1.7 V), it could be used to convert low-frequency vibrational mechanical energy from daily-life activities.

Structure engineering (or geometry innovation) is also an important factor to extend PENG to different application scenarios. For instance, Ryu et al. developed an intrinsically stretchable versatile hollow fiber-shaped PENG (Figure 3d).[60] Han et al. reported a piezoelectric helical nanobelt composed of P(VDF-TrFE), graphene, and multiwalled carbon nanotube (MWCNT) by the direct-write technique (Figure 3e).[61] These devices could collect energy from diverse external mechanical stimuli and showed potential in the field of wearable and robotic applications. Another work developed hierarchically structured PVDF/ZnO core–shell nanofibers for PENG (Figure 3f),[62] which displayed great electrical performance and high flexibility, thus providing a substitutable strategy for monitoring the human physiological signals.
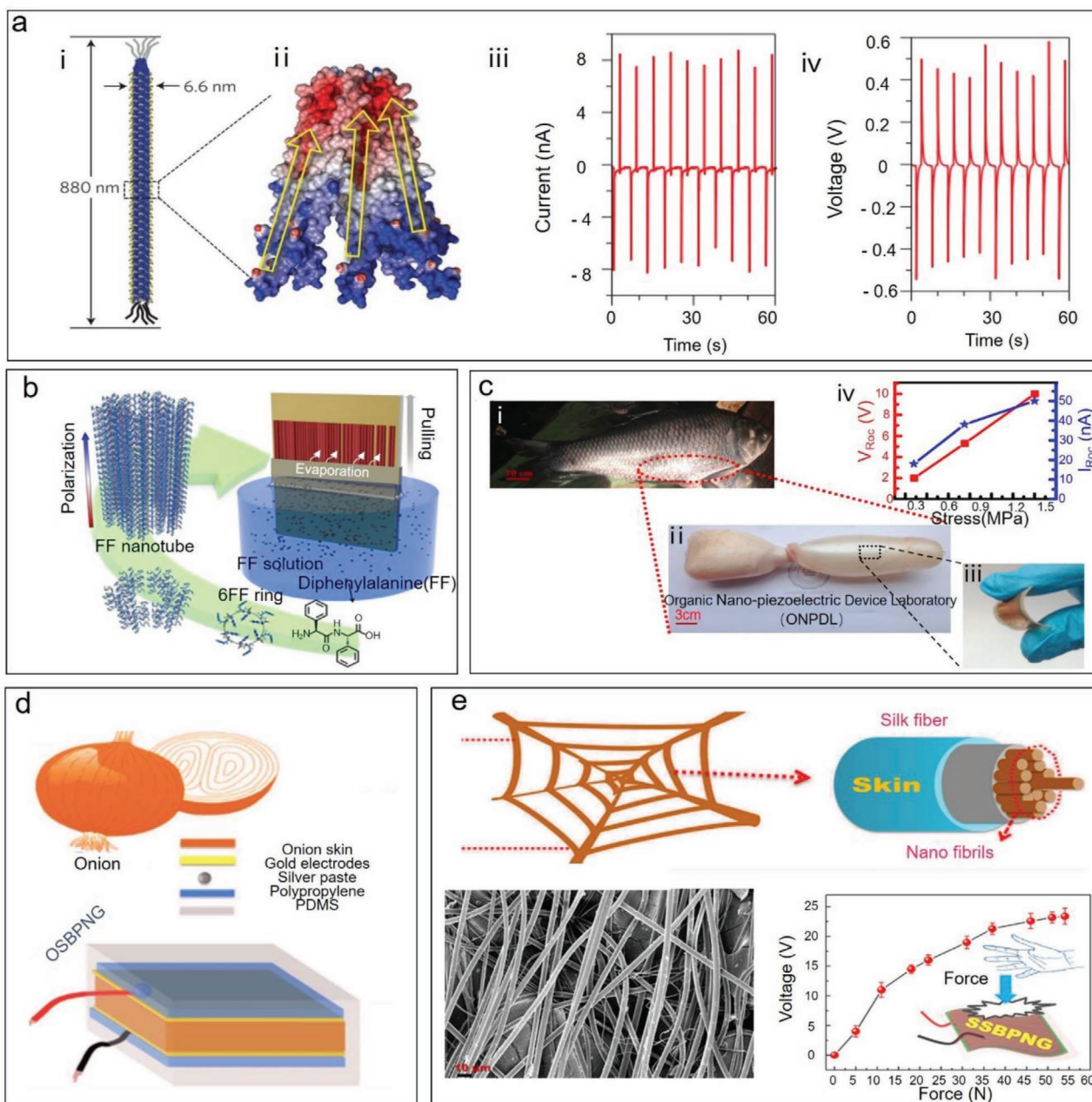
2.1.3. Biopiezoelectric Materials

The naturally abundant biological tissues, microorganisms, and biodegradable biomaterials were also reported to have good piezoelectricity.[63–65] With the development of biotechnology, the biopiezoelectric materials potentially provided a simple and environmentally friendly method for energy harvesting. In recent years, there have been plenty of studies about PENGs based on biomaterials, such as virus,[65] peptides,[66] fish scale,[67] and cellulose nanofibril.[68,69] However, the reported PENGs showed low power density due to the intrinsically weak piezoelectricity of biomaterials. They are more suitable for short-term, disposable, and even biodegradable applications owing to the excellent biocompatibility of biomaterials.

Lee et al. demonstrated the piezoelectricity of M13 bacteriophage and developed a phage-based PENG to generate electrical energy (**Figure 4**a-I).[65] The output performance of the PENG based on M13 bacteriophage is shown in Figure 4a-III,IV, exhibiting an I_{SC} up to 6 nA and a V_{OC} up to 400 mV under the operation of a liquid crystal display (LCD). Lee et al. reported aligned and unipolarized piezoelectric peptide nanotubes and fabricated peptide-based PEH.[66] They successively fabricated horizontally aligned nanotubes via the meniscus-driven self-assembly process (Figure 4b). It generated 2.8 V of voltage, 37.4 nA of current, and 8.2 nW of power under applied force at 42 N, which could power multiple LCD panels. Natural piezoelectric materials such as collagen fibrils are also known as environmentally friendly material and offer a suitable choice for the preparation of biopiezoelectric nanogenerators (Bio-PENG). Collagen has three polypeptide chains, which twists together into a unique triple helix structure. The polar uniaxial orientation of hydrogen bonds between polypeptide chains is molecular dipole, which leads to spontaneous polarization and piezoelectricity. It also makes

collagen a natural electret or biological electret material.[70–72] Collagen is one of the rich tissue components of fish. Ghosh et al. collected the fish scales from the seafood market and demonstrated an effective Bio-PENG, where the "biowaste" fish scale served as a natural piezoelectric component.[70,73] The origin of piezoelectricity in fish scale was attributed to the highly stable crystalline structure of polypeptide chains of collagen and strong degree of molecular alignment (19%) of −CONH hydrogen bonding motif. The fish scales collagen based Bio-PENG could harvest energy from ambient mechanical energies such as body movements, machine and sound vibrations. It generated an I_{SC} of 1.5 μA, a V_{OC} of 4 V and the ultimate output power density of 1.14 μW cm^{-2} with repeatable compressive stress of 0.17 MPa. They had also fabricated a Bio-PENG from the fish swim bladder (Figure 4c-I,II), which was composed of naturally well-aligned collagen nanofibrils.[74] Collagen nanofibrils have very strong degree of molecular alignment of maximum 13% and highly orientational ordering of the amide bond, which determine the excellent piezoelectric strength ($d_{33} \approx 22$ pC N^{-1}) of collagen material. When they are used to prepare for a Bio-PENG, it can generate a V_{OC} of 10 V, an I_{SC} of 51 nA, and instantaneous piezoelectric power generation of the excellent power density of 4.15 μW cm^{-2} (Figure 4c-I,ii,iv). Due to the biocompatibility of the collagen fibril, it can be not only used as an energy harvester, but also expected to work as an active biomedical sensor to monitor physiological signals such as heartbeat and blood circulation.

Another important biopiezoelectric material is cellulose with intermolecular hydrogen bond formed in collagen chains to induce uniaxial orientation of molecular dipoles. It is enriched in most of the plants and plays a crucial role in developing piezoelectric devices.[75,76] Zhang et al. proposed a flexible paper-based PENG with bacterial cellulose (BC) produced by *Gluconacetobacter*.[69] Bacterial cellulose had good mechanical strength and flexibility.[77] Compared with the plant cellulose, BC represented the purest form of cellulose, which had no residual contaminants such as lignin and hemicellulose.[78] The paper-based PENG with BTO/BC generated a voltage of 1.5 V and a power density of 0.64 μW cm^{-2} to successfully drive a commercial LCD screen. However, it showed relatively low power density. Maiti et al. used naturally abundant onion skin (OS) to develop an innovative Bio-PENG with flexible, biodegradable, low-cost and biocompatible for energy scavenging in various in vivo applications (Figure 4d).[79] The surface of the onion skin had regularly and naturally aligned microfibrils, the good ferroelectric property and large remanent polarization (P_r) of 0.053 μC cm^{-2} determined its piezoelectricity. Onion skinbased PENG showed a higher performance with power density of 1.7 μW cm^{-2} and higher piezoelectric energy conversion efficiency of 61.7% compared with paper-based PENG with bacterial cellulose. Onion skin-based PENG could instantly light up 30 green LEDs by a single device and effectively drive commercial calculator, electronic watch, and portable electronic displays.

As early as 1939, Harvey found the reddish luminescence after shaking of silk fragments, which was attributed to the intrinsic piezoelectricity of silk.[80] Intrinsically, the crystalline regions in semicrystalline fibroin fibers assume a β-sheet secondary structure. The combination of β-sheet crystallinity

ADVANCED
SCIENCE NEWS
www.advancedsciencenews.com

ADVANCED
FUNCTIONAL
MATERIALS
www.afm-journal.de

Figure 4. a-I) The M13 phage is ≈880 nm in length and ≈6.6 nm in diameter, is covered by ≈2700 pVIII coat proteins, and has five copies each of pIII (gray lines) and pIX (black lines) proteins at either end. II) Side view of the electrostatic potential of M13 phage after bioengineered modification with four glutamate amino acids. III) Short-circuit current and IV) open-circuit voltage of phage-based generators. Reproduced with permission.[65] Copyright 2012, Macmillan Publishers Limited. b) Schematic diagram depicting the fabrication process to create large-scale peptide nanotube arrays through the meniscus-driven self-assembly. Reproduced with permission.[66] Copyright 2018, American Chemical Society. c) Piezoelectric nanogenerator based on swim bladder. The photograph of the I) sweet water fish and II) swim bladder. III) The flexibility of the fish swim bladder (FSB) with sputtered Au electrodes. IV) Output voltage and current from the BPNG by different stresses. Reproduced with permission.[74] Copyright 2016, Elsevier Ltd. d) Schematic of structure of OSBPNG with cross-section view. Reproduced with permission.[79] Copyright 2017, Elsevier Ltd. e) Schematic of spider silk structure and fibril type of a single spider silk, SEM images of natural spider silk, and the output voltage generation of SSBPNG subjected to pressure. Reproduced with permission.[82] Copyright 2018, Elsevier Ltd.

and crystal orientation is a prerequisite for the generation of strong piezoelectric effect in silk.[81] Karan et al. reported a Bio-PENG based on the biodegradable spider silk for energy harvesting and smart sensing (Figure 4e),[82] representing a force-dependent output voltage that increased with the growing

applied force. The fabricated spider silk-based Bio-PENG showed a high V_{OC} of 21.3 V and a maximum instantaneous power density of 4.56 µW cm^{-2}, which are the maximum values of Bio-PENGs among all the literature. The device is also readily utilized for physiological signal monitoring, such

**ADVANCED
SCIENCE NEWS**
www.advancedsciencenews.com

**ADVANCED
FUNCTIONAL
MATERIALS**
www.afm-journal.de

Table 2. The performance and applications of piezoelectric nanogenerators based on different piezoelectric materials.

	Piezoelectric materials	Voltage	Current	Application	Material category
Lee et al.[83]	ZnO nanowire arrays	50 mV	20 nA	PEH, sensor	Inorganic crystal
Hasan Ul Banna and Park[84]	ZnO nanorod	3.6–6.8 V	0.79–1.45 μA	PEH	Inorganic crystal
Lin et al.[85]	GaN nanowire	1.2 V		PEH	Inorganic crystal
Wu et al.[25]	Single-atomic-layer MoS_2	15 mV	20 pA	Piezotronics	Inorganic crystal
Xue et al.[31]	2D α-In_2Se_3	35.7 mV	47.3 pA	PEH, sensor	Inorganic crystal
Han et al.[86]	2D MoS_2 shell arrays	1.2 V		PEH	Inorganic crystal
Niu et al.[87]	$Pb(Zr_{0.52}Ti_{0.48})O_3$	65 V	1 μA	PEH	Inorganic ceramic
Jian et al.[37]	$BaTiO_3$ flowers	260 V	50 μA	PEH	Inorganic ceramic
Yu et al.[38]	$BaTiO_3$ particles	8.9 V	49.7 nA	PEH	Inorganic ceramic
Ryu et al.[60]	P(VDF-TrFE)	1.2 V	10 nA	PEH	Piezoelectric polymer
Han et al.[61]	PVDF–TrFE nanobelts	10.3 mV		PEH	Piezoelectric polymer
Karan et al.[88]	Fe–RGO/PVDF	5.1 V	0.254 μA	PEH, sensor	Nanocomposite
Zhao et al.[59]	MnO_2/PVDF	3.2 V		PEH	Nanocomposite
Yang et al.[62]	PVDF/ZnO core–shell nanofibers	1.5 V		Sensor	Nanocomposite
Pal et al.[53]	PZT/MWCNT/PVDF	20 V	250	PEH	Nanocomposite
Lee et al.[65]	M13 bacteriophage	400 mV	6 nA	PEH	Biopiezoelectric
Lee et al.[66]	Ddiphenylalanine (FF) nanotubes	2.8 V	7.4 nA	PEH	Biopiezoelectric
Ghosh and Mandal[74]	Fish swim bladder	10 V	51 nA	PEH, sensor	Biopiezoelectric
Ghosh and Mandal[73]	Fish scale	4 V	1.5 μA	PEH	Biopiezoelectric
Maiti et al.[79]	Onion skin	18 V	166 nA	PEH, sensor	Biopiezoelectric

as arterial pulse response, which is very useful for potential biomedical applications. **Table 2** shows the different performance and applications of piezoelectric nanogenerators based on piezoelectric materials. We can choose suitable materials according to our needs, such as biocompatibility, compressive strength, output performance, etc.
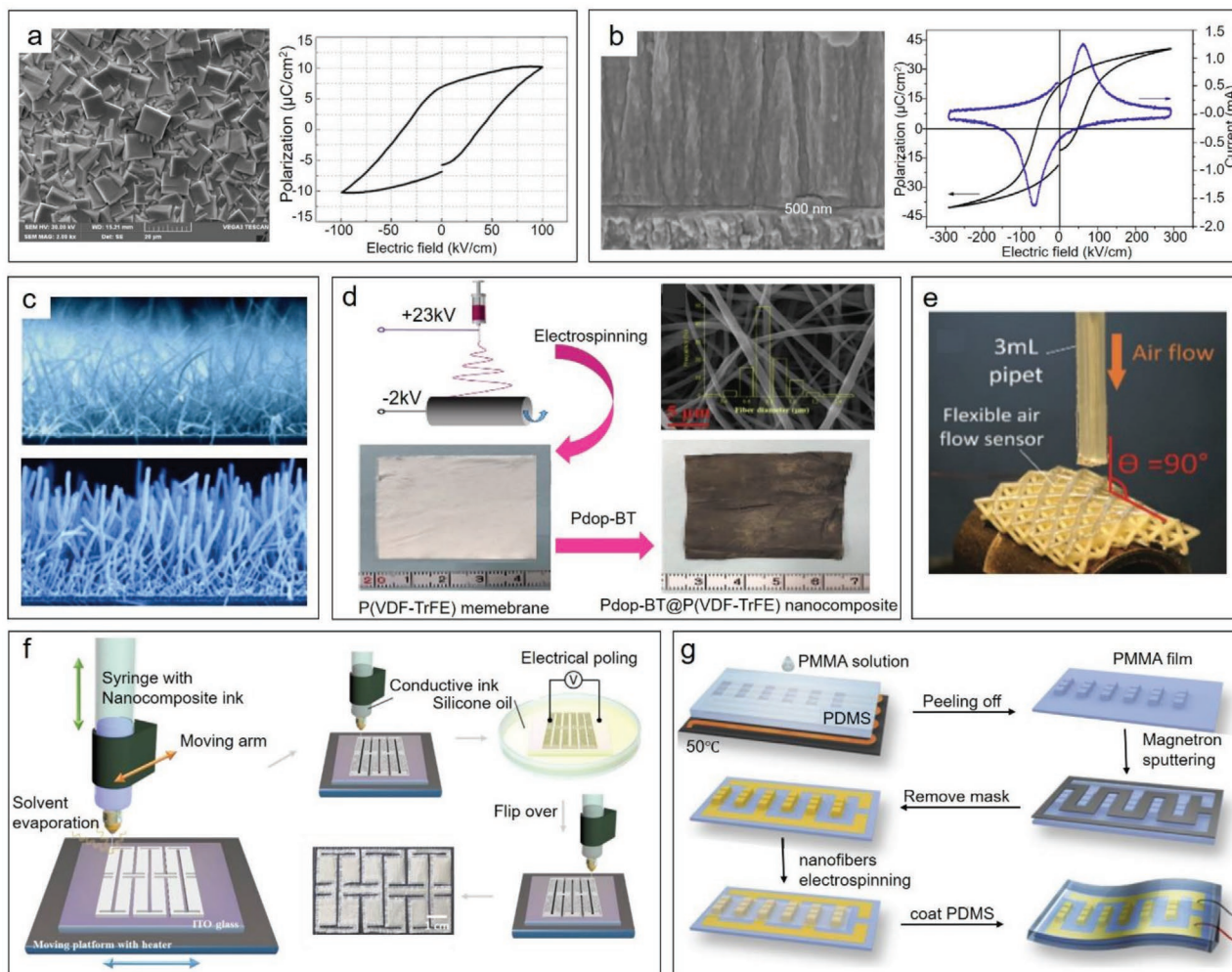
2.2. Processing

The preparation process for the piezoelectric material has a significant impact on device performance. With the increased requirements for piezoelectric performance in intelligent sensors and self-powered systems, studies on how to process the piezoelectric materials have been continuously developed, which will also reversely promote new research and development of piezoelectric materials. In recent years, various fabrication techniques have been developed to utilize superior piezoelectric materials in energy harvesters and piezoelectric sensors with constantly improved output performance.

The hydrothermal and sol–gel methods are commonly used to synthesize typical inorganic piezoelectric materials of PZT and ZnO.[89–94] The sol–gel method shows advantages in precision control and economical, while the hydrothermal method has the minimum synthesis temperature (≤200 °C),[95] which are both effective to fabricate PZT thick films. Instead of conventional hydrothermal equipment (a large-scale autoclave with integrated stirring equipment), Wang et al. used an innovative and economical hydrothermal method based on oil-bath to successfully synthesize the PZT thick films (10 μm) with

good piezoelectricity (**Figure 5**a).[96] Thick PZT ferroelectric films were also prepared through a sol–gel process on Ti–Pt/Ti/SiO$_2$/Si (100) alloy substrates.[97] As shown in Figure 5b, dense columnar grains are observed in the PZT film with high piezoelectricity, the preferential crystal orientations of which increases with the increased content of Ti in the alloy substrate. In addition to hydrothermal and sol–gel methods, some other methods (such as screen, tape casting, radio frequency (RF) magnetron sputtering, etc.[98–100]) have also been developed to prepare PZT thick films. For example, Wu et al. prepared high-quality oriented ZnO thin films on Al_2O_3 substrates by the rapid hydrothermal method, in which RF assisted molecular beam epitaxy (MBE) deposition on ZnO buffer layers.[101] The film prepared with the precursor concentration of 0.05 mol L^{-1} showed smooth and homogeneous morphology. More methods have also been reported to grow high-quality ZnO films, such as CVD,[102] pulsed laser deposition (PLD),[103] electrochemical deposition (ECD),[104] and magnetron sputtering.[105] As shown in Figure 5c, Filippin et al. presented a combined vacuum and plasma deposition method for the formation of core–multi-shell nanowires.[106] Single-crystal organic nanowires deposited in vacuum provided a reliable 1D core for plasma deposition of piezoelectric ZnO shells. Conformal plasma deposition on organic nanowires resulted in ZnO shells composed of tightly packed and aligned nanorods, which were conformally coated on the surface of nanowires.

For piezoelectric polymer materials such as PVDF and its copolymer P(VDF-TrFE), electrospinning is extensively used to prepare piezoelectric nanofibers in addition to conventional tape casting and spin-coating methods.[107] Electrospinning is

**ADVANCED
SCIENCE NEWS**
www.advancedsciencenews.com

**ADVANCED
FUNCTIONAL
MATERIALS**
www.afm-journal.de

Figure 5. a) SEM photographs and ferroelectric hysteresis loop of PZT thick film. Reproduced with permission.[96] Copyright 2017, Elsevier Ltd. b) Cross-sectional images of the PZT films and Ti–Pt alloy layers, Ti–Pt alloy layers with various sputtering power typical P–E hysteresis curves, and switching current loops of the sample. Reproduced with permission.[97] Copyright 2020, Elsevier Ltd. and Techna Group S.r.l. c) SEM micrographs of core–multishell supported nanowires. Reproduced with permission.[106] Copyright 2019, Elsevier Ltd. d) Schematic of electrospinning process and the SEM images of as-electrospun P(VDF-TrFE) nanofiber membrane, digital photograph of as-electrospun mat, and Pdop-BT@P(VDF-TrFE) nanocomposite. Reproduced with permission.[109] Copyright 2020, Elsevier Ltd. e) Optical image of the conformal flexible air flow sensor with air flow applied in 90°. Reproduced with permission.[111] Copyright 2019, Wiley-VCH GmbH. f) Schematic of the fabrication process of the all 3D-printed PENG. Reproduced with permission.[112] Copyright 2020, The Authors. Published by Elsevier Ltd. g) The process of fabricating piezoelectric nanogenerator based on 3D interdigital electrodes. Reproduced with permission.[114] Copyright 2019, Elsevier Ltd.

an effective method to convert the common α-phase of PVDF into piezoelectric β-phase due to the high electric field and polymer jetting characteristics during the in situ electric poling and mechanical stretching process. Koç et al. prepared aligned PVDF nanofibers doped with different volumes of PZT by a rotating drum collector via the electrospinning method.[108] They also increased the β-phase content in the resulting PVDF/PZT nanofibers by using the alignment method to strengthen the capacity of PEHs. Guan et al. prepared P(VDF-TrFE) membrane via electrospinning technology to construct a nanofiber network for nanoparticle adsorption (Figure 5d),[109] and functionalized the BaTiO$_3$ nanoparticles by in situ polymerization via polydopamine. The PENG based on the prepared nanocomposite exhibited excellent flexibility, significantly enhanced piezoelectricity, and durability.

To fabricate PENGs with desired geometry and dimensions, 3D printing or additive manufacturing has recently been developed.[110] As shown in Figure 5e, Yao et al. presented a novel method for a 3D printable and wearable flexible piezoelectric nanocomposite.[111] They used trialkoxysilane-methacrylate functionalized PZT as the active material to maximize piezoelectric responses. Zhou et al. fabricated a stretchable Kirigami-structured PENG composed of BaTiO$_3$ nanoparticles, P(VDF-TrFE) matrix, and silver flake-based electrode through an all-3D printable process.[112] Figure 5f shows the schematic of the fabrication process of all 3D-printed PENG. Through the Kirigami strategy, the PENG device achieved high stretchability and demonstrated its great potential in wearable flexible and stretchable energy harvesting systems.

Moreover, the preparation process of PENG electrodes is also an important research concern. Highly efficient utilization of

**ADVANCED
SCIENCE NEWS**

www.advancedsciencenews.com

**ADVANCED
FUNCTIONAL
MATERIALS**

www.afm-journal.de

space and flexible micro/nanoscale piezoelectric sensors can be achieved through the interdigital electrode structure. Zhuang et al. prepared the interdigital electrode pattern by using the lithography method and then fabricated a flexible interdigital-structured nanosensor with excellent performance.[113] As shown in Figure 5g, Zhang et al. designed the flexible PENG based on P(VDF-TrFE) nanofibers with micropatterned 3D interdigital electrodes.[114] First, they fabricated micropatterned PDMS using standard photolithography and soft lithography techniques. Then, the polymethyl methacrylate (PMMA) solution was coated on the PDMS substrate and peeled off after annealing. The Au interdigital electrodes were formed on the patterned PMMA film by magnetron sputtering. The micropatterned 3D interdigital electrodes enhanced the modulus of nanofibers and optimized the performance of PENGs, showing big potential in fabrication of flexible self-powered sensors.

2.3. Performance Enhancement

A typical wurtzite-structured semiconductive piezoelectric material is ZnO, which has been used to develop the first ZnO NW-based PENG by Z. L. Wang. The achieved output voltage at the beginning of the PENG invention was ≈9 mV. After that, gallium nitride (GaN),[85] PZT,[115,116] and lead-free $BaTiO_3$ nanoparticles[117,118] were successfully used to prepare different types of PENGs for various applications. These piezoelectric materials generated certain output voltages and currents. However, they were relatively low and could not truly meet the energy requirements of microelectronic devices. Over years, many attempts have been made to achieve high-performance PENGs, with the output voltage increased from the initial millivolt range to 100 V. Meanwhile, PENG has also been greatly improved in the output current, targeting at directly driving portable microelectronic devices. Until now, how to enhance the output performance of PENGs and develop more sophisticated applications is still an important research topic. In this part, we classify the PENG performance enhancement methods into three categories, including chemical doping of piezoelectric materials, preparing piezoelectric materials into aligned nanofibers, and engineering on interfacial modification.

2.3.1. Performance Enhancement with Chemical Doping

PENGs based on different piezoelectric materials (e.g., ZnO, PZT, $BaTiO_3$, and PVDF) have specific and different applications, but the performance still needs to be improved. Researchers have proposed an effective strategy for chemically doping piezoelectric materials to modify the piezoelectric coefficients and dielectric constants. Readily tunable energy harvesting properties can be achieved by chemical doping with different chemical dopants.[119–124]

Generally, the doping strategy for ZnO is classified into n-type and p-type doping. For n-type doping, the dopant can decrease crystal lattice strain along the polar c-axis of the ZnO crystal, increase the piezoelectric coefficient, and improve the output performance of the PENGs. p-Type doping can reduce the shielding effect of the free electrons generated by

the dopant in the ZnO nanowires. Metal,[125–128] rare earth (RE) metal,[129–132] and nonmetallic elements (such as S ions[133] and halogen ions[119,134]) have been used as dopants to achieve ZnO PENGs with improved piezoelectric properties and high performance. As shown in **Figure 6**a, Batra et al.[135] fabricated pure and Tb-doped ZnO NPs via chemical coprecipitation technique, and the doping effect of Tb^{3+} on the structural and electrical properties of ZnO NPs was studied. It was found that hexagonal structured pure ZnO nanorods were converted to taper-like nanoparticles after doping. Simultaneously, it showed a high Curie temperature (T_c ≈ 225 °C) and enhanced dielectric constant. Compared with common piezoelectric properties based on Zn–O bonds, the enhanced piezoelectric outputs were attributed to the higher polarity of Tb–O bonds, which exhibited easier orientation of bonds under applied external field. Then, the Tb-doped ZnO NPs/PDMS composite was prepared on flexible ITO/PET substrate with Al/PES as the other electrode to fabricate the PENG in a piezoelectric sandwich structure. Under the external pressure of 2 kgf, a high and stable piezoelectric V_{OC} of ≈9.0 V was obtained for Tb-doped ZnO PENG, which was attributed to that the doping of Tb could help to reduce the piezoelectric shielding effect. Similarly, halogen ions play an indispensable role in modulating lattice strain along the ZnO polar c-axis. For F^--doped ZnO nanowires, as the radius of F^- is slightly smaller than the radius of O^{2-}, the induced compressive strain within the crystal structure will inhibit the output performance. In contrast, the radius of Cl^-, Br^-, and I^- are all larger than that of O^{2-}. Doping with these halogen elements will induce the expansion strain generated along the c-axis of the ZnO lattice to increase the stress strain and improve the performance of the PENGs. Zhang et al. demonstrated an efficient strategy for employing halogen elements (chlorine, bromine, and iodine) as a dopant to strengthen the output performance of ZnO-based PENGs,[134] and **Table 3** shows the ZnO lattice strain dependence of the output performance of PENG.

ZnO and other inorganic piezoelectric materials usually have higher d_{33} values than piezoelectric polymers, but they are too rigid and fragile to be directly used for constructing flexible devices. The synthesis of the chemical-doped inorganic piezoelectric materials into the piezoelectric polymer matrix (e.g., PVDF and its copolymers) can not only significantly improve the piezoelectric properties of the composites but also maintain their flexibility.[88,136–138] Jin et al. developed a small-size PENG based on a composite of metal-doped ZnO NPs distributed in porous P(VDF-TrFE) matrix,[138] which showed enhanced piezoelectricity and energy conversion efficiency. The authors also carried out a systematic and direct comparison to reveal the different energy-harvesting properties based on various metal dopants (such as Co, Ag, Na, and Li) and doping concentrations. As shown in Figure 6b, they identified that the 5% Li-doped device was improved with the output voltage nine times higher than a pure ZnO PENG. Moreover, this device could be used to power small electronics by harvesting biomechanical energy and functionalized as a flexible wearable motion sensor to detect human body motions. Karan et al. also reported a flexible, low-price, light-weight Fe-doped graphene oxide/PVDF (Fe-RGO/PVDF) piezoelectric nanocomposite by a solution casting method.[88] As Fe–RGO has an excellent ability
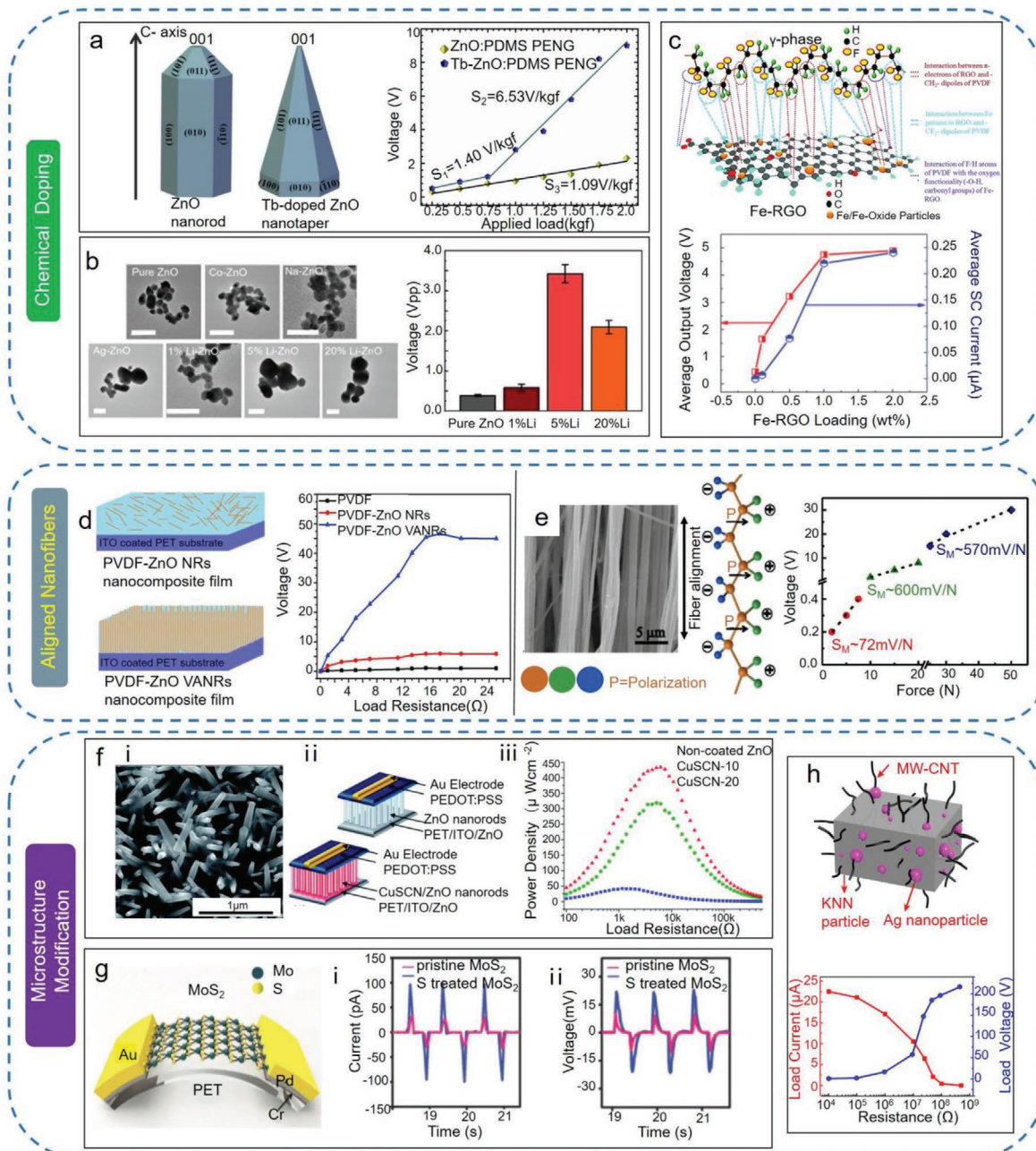
Figure 6. Ways to enhance output performance of PENGs. a) Schematic representation of various planes in ZnO nanorods, Tb–ZnO nanotaper, and open-circuit output voltage generated from 30 wt% synthesized ZnO nanoparticle-based PENGs under 1 Hz and different applied loads. Reproduced with permission.[135] Copyright 2020, Elsevier Ltd. and Techna Group S.r.l. b) TEM image of pure, Co, Na, Ag, and 1%, 5%, and 20% Li-doped ZnO nanoparticles. The scale bar is 500 nm and the average voltage output for devices with 1%, 5%, and 20% Li-doped ZnO nanoparticles. Reproduced with permission.[138] Copyright 2020, Elsevier B.V. c) Proposed schematic illustration showing the interaction between the γ-phase of PVDF and an Fe–RGO nanosheet facilitating the γ-phase formation within the polymer nanocomposite. The output voltage and short-circuit currents shown as a function of the Fe–RGO filler loading in PVDF. Reproduced with permission.[88] Copyright 2015, The Royal Society of Chemistry. d) Schematic diagrams of PVDF–ZnO NRs and PVDF–ZnO VANRs nanocomposite films, and open-circuit voltage with different load resistances. Reproduced with permission.[141] Copyright 2019, Elsevier Ltd. e) FE-SEM image of aligned arrays of Pt–PVDF NFs along the surface direction with their polarization direction along the thickness direction (shown schematically) and linear relationship and sensitivity of voltage with applied force at a constant frequency of 5 Hz. Reproduced with permission.[149] Copyright 2018, Elsevier Ltd. f-I) SEM images of the CuSCN-coated samples. II) Schematics of noncoated and CuSCN-coated device. III) Resistive load match measurements performed from 100 Ω to 550 kΩ. Reproduced with permission.[160] Copyright 2014, The Royal Society of Chemistry. g) Schematic of the PENG based on monolayer MoS_2 nanosheets. I) Output current and II) voltage difference between the pristine and S-treated monolayer MoS_2 PENGs. Reproduced with permission.[161] Copyright 2018, Wiley-VCH GmbH. h) Schematic diagram of KNN particles, Ag nanoparticles, and MW-CNTs distribution in PDMS matrix. Output voltage and current dependence on the load resistance at a frequency of 1 Hz and a compressive stress of 0.1 MPa for the 3% Ag p-NG device. Reproduced with permission.[165] Copyright 2018, Elsevier Ltd.

**ADVANCED
SCIENCE NEWS**
www.advancedsciencenews.com

**ADVANCED
FUNCTIONAL
MATERIALS**
www.afm-journal.de

Table 3. ZnO lattice strain dependence of the output performance of piezoelectric nanogenerator.[134]

	ZnO	ZnO:F	ZnO:Cl	ZnO:Br	ZnO:I
Lattice strain [%]	0	−0.035	0.3	0.45	0.16
Voltage [V]	2.8	2.6	4.9	5.9	4.7
Current density [nA cm^{-2}]	380	355	1140	1850	1055

of facilitating the nucleation and stabilization of electroactive γ-phase, the relative proportion of γ-phase will gradually increase with the increased load concentration of Fe–RGO. Accordingly, an almost complete transformation (≈99%) of the γ-phase can be achieved by controlling the filler concentration (≈2 wt%). Figure 6c shows that the human finger touch-induced output voltage by the Fe–RGO/PVDF nanocomposite film exhibits a V_{OC} of 5.1 V and I_{SC} of 0.254 A, which are 12 times and 105 times higher than that of pure PVDF, respectively.

2.3.2. Performance Enhancement with Aligned Nanofibers

Manufacturing PENGs with highly aligned piezoelectric nanofibers is another efficient way to enhancing output performance. The parallel alignment of dipoles can lead to more effective surface charge separation for an enhanced piezoelectric response.

PENGs based on the 2D ZnO nanosheets with aligned ZnO nanowires by two-step hydrothermal method has shown superior output performance than those based on 1D ZnO NWs, with output current surprisingly increased from ≈40 nA to ≈0.15 μA under the same compressive stress.[139] Yang et al. obtained a piezoelectric composite with higher breakdown strength and enhanced piezoelectric properties by incorporating highly aligned TiO$_2$@MWCNTs in the PVDF matrix.[140] Anand and Bhatnagar compared flexible and cost-effective PENGs based on two solution-casted nanocomposites (ZnO nanorods and vertically aligned ZnO nanorods distributed in PVDF films).[141] The value of remanent polarization was enhanced after aligned ZnO nanorods were added into PVDF, thus orienting all the molecular dipoles and exhibited a stronger electric field. As shown in Figure 6d, the output voltage and short circuit current for aligned ZnO/PVDF are 46.64 V and 1.392 μA, respectively, seven times more than those of the counterpart based on ZnO/PVDF. This result reveals that the preparation of aligned piezoelectric materials can strengthen the output performance of PENGs. Ye et al. fabricated an innovative PENG based on nanocomposite micropillar arrays composed of P(VDF-TrFE)/boron nitride nanotubes (BNNTs).[142] It surprisingly enhanced the output performance and excellent neutron radiation shielding properties. The device showed a high V_{OC} of 22 V and a sensitivity of 55 V MPa^{-1} with the applied force at 0.4 MPa. These values are 11 times higher than those of the pure P(VDF-TrFE) film.

The piezoelectric polymers, e.g., PVDF and (PVDF-TrFE), generally have five semicrystalline polymorphs (introduced in Section 2.1.2), which depend on their macromolecular chain orientation of *trans* (*T*) and *gauge* (*G*) linkages.[50] The level and orientation of β-phase and degree of crystallinity are the key factors influencing the piezoelectric response of PVDF. Therefore,

increasing the concentration of β-phase in PVDF becomes one of the most effective strategies to strengthen piezoelectric response. First, the fibers can be efficiently crystallized in the β-phase when processed into aligned fibers via electrospinning.[49,140,143,144] Second, the electrospinning process not only helps to crystallize the polymer, but also effectively polarizes the inorganic fillers, which is conducive to the induction of charges to increase the output performance.[145,146] Furthermore, coaxial-structured nanofibers with 1D nanofillers can also be fabricated by electrospinning, which significantly improved performance due to the synergistic effect between the aligned fillers and matrix. For instance, the synergistic effect between MWCNTs and P(VDF-TrFE) have an enhanced output performance. This is because 1D CNTs with high aspect ratio are easier to form a radial array structure and strengthen the crystallization of P(VDF-TrFE) during the electrospun process.[122,123] In addition, MWCNTs can trap free charges injected during electrospinning and gather them at the interfaces. The bound charges will contribute to the polarization inside the nanofibers composite by inducing more dipoles and lead to increased number of the inductive charges on the outside surfaces of the nanofiber. Zhao et al. prepared flexible fibrous membranes via electrospinning.[147] The PENG constructed with 3 wt% of aligned MWCNTs generated a high V_{OC} of 18.23 V and I_{SC} of 2.14 μA. The output power density was evaluated to be 6.53 μW cm^{-2} with a load resistance of 10 MΩ.

Chen et al. achieved a high β-phase concentration in the PVDF nanofiber film doped with BiCl$_3$ by electrospinning, which also enhanced the piezoelectric power output.[148] Ghosh and Mandal developed an all-fiber wearable PENG, where the piezoelectric active layer with platinum nanoparticles precipitated on highly aligned 1D PVDF nanofiber arrays was sandwiched between flexible conducting fabrics.[149] The aligned 1D nanofibers with precipitated Pt-NPs resulted in the enhancement of β-phase (≈99.9%) and a 75% degree of fiber alignment. With highly aligned Pt–PVDF nanofibers, the device generated an excellent performance with an output voltage of 30 V and current density of ≈6 mA cm^{-2}. It also showed superior mechanosensitivity, becoming suitable for wearable nanotactile sensors (Figure 6e).

2.3.3. Performance Enhancement with Surface Modification Engineering

The piezoelectric properties of piezoelectric materials are related to their microscopic morphology, and greatly affect the performance of the fabricated PENGs. This is because the surface micro/nanostructures with a higher surface-to-volume ratio can help to increase the trapping points for charge transfer to improve the output performance. In general, the performance

ADVANCED
SCIENCE NEWS
www.advancedsciencenews.com

ADVANCED
FUNCTIONAL
MATERIALS
www.afm-journal.de

Table 4. The performance of piezoelectric materials with different micromorphologies.

Materials	Micromorphologies	Voltage	Current
ZnO	Nanorod[152]	9.5 mV	–
	Nanowire[153]	2.03 V	107 nA
	Nanosheet[151]	30 mV	0.2 µA
BaTiO$_3$	Nanotube[154]	5.5 V	350 nA
	Nanowire[155]	7.0 V	360 nA
	Nanopillar[36]	6.0 V	0.8 µA
PZT	Nanowire[156]	10 V	1.2 µA
	Nanorod[34]	3.3 V	–
	Nanofiber[157]	1.63 V	–

of PENG fabricated by ZnO nanorods is weaker than that of ZnO nanowires,[150] and 2D ZnO nanosheets obtained because of the high surface-to-volume ratio had the better current than 1D ZnO nanowires.[151] In contrast, PENGs based on BaTiO$_3$ and PZT with different micromorphologies had different performances. **Table 4** compares the performance of piezoelectric materials with different micromorphologies. Thus, it is a promising way to prepared PENGs with high output performance by changing the micromorphology of piezoelectric materials.

On the other hand, due to the low-temperature characteristic of the hydrothermal method for ZnO synthesis, the intrinsic defects such as oxygen vacancies and surface-related defects such as absorbed water induce a large number of free charge carriers in ZnO lattice, which will inevitably weaken the performance. Therefore, to further strengthen the output performance of PENGs, various strategies (e.g., oxygen plasma treatment, surface passivation, and interfacial modification) have been attempted to weaken the above mentioned defects and enhance the performance of energy harvesting devices.

Oxygen plasma technique could suppress surface accumulation layer and oxygen vacancies by producing oxygen radical atoms (O·), which can then combine with absorbed hydrogen atoms and defuse via ZnO bulk to fill in these oxygen vacancies. Hussain et al. developed a flexible PENG on the monolayer graphene-coated PET substrate based on oxygen plasma-treated ZnO nanorods.[158] Oxygen plasma treatment helps to improve the average output from 78 to 122.7 mV. Nevertheless, the plasma treatment effect on ZnO is not very stable under environmental conditions.

Surface passivation offers a more effective and stable method to modify nanostructures. The PENG performance can be greatly improved by a stepped treatment of the ZnO NW arrays with oxygen plasma, thermal annealing, and surface passivation with polymers. The maximum output voltage reaches 20 V based on a single layer of ZnO nanowire, which is 20 times larger than that of the previously reported best PENG.[159] Jalali et al. also demonstrated a surface modification method to improve the power density of ZnO nanorod-based PEHs via reducing the surface-state-induced parasitic losses.[160] As shown in Figure 6f, the device with surface modification generated a V_{OC} of 1.07 V and a power density of 434 µW cm^{-2} upon dropping load at an acceleration of 50 g.

Han et al. proposed a high-performance PENG based on point-defect-passivated MoS$_2$ nanosheet.[161] Figure 6g shows the schematic of the MoS$_2$-based PENG, which consists of monolayer MoS$_2$ nanosheet and Au electrodes on the PET substrate. The S vacancies were effectively passivated and the charge-carrier density was reduced after treatment of S element on the pristine MoS$_2$ surface. As a result, the output peak current and voltage of the S-treated monolayer MoS$_2$ PENG were increased by more than 3 times (100 pA; Figure 6g-I) and 2 times (22 mV; Figure 6g-II), respectively. Furthermore, the S treatment process increased the maximum power by almost 10 times.

In the case of ZnO NWs subject to an external force, inherent polarization appears inside the nanowire and leads to positive and negative charges on the opposite surface of the nanowire,[162] thereby generating a piezoelectric potential. The piezoelectric potential drives electrons to flow through an external circuit and results in a piezoelectric output. Meanwhile, the piezoelectric field can also drive the charge carriers to migrate inside ZnO, which partially screens the piezoelectric field and inversely reduces the piezoelectric output.[163] Therefore, interfacial modification method has been attempted to improve piezoelectric output performance via reducing both internal and external screening effects. Yin et al. reported the first example of interfacial modification by constructing a NiO–ZnO heterostructure,[164] which had a depletion region near the junction boundary. Therefore, the built-in electric field near the junction boundary effectively depletes excess electrons in the ZnO layer and reduces the screening effects for the generated piezoelectric potential. This results in 21 times higher output voltages and over 10 times higher output currents compared with the pristine samples. Huan et al. introduced an Ag/(K, Na)NbO$_3$ (Ag/KNN) heterostructure to fabricate PENG,[165] the chemical heterojunction of which improved the part of voltage applied to the KNN particles during the polarization process and thereby vastly improved the dipole moment orientation. As shown in Figure 6h, the PENG device with Ag/KNN heterostructure obtained a 240 V of the V_{OC} and 23 µA of the current, which were two orders of magnitude higher than those of the pure KNN-based device.

3. Prerequisite Energy Harvesting

During the last ten years, PENGs have attracted intensive attention for readily collecting energy from various mechanical actions. The piezoelectricity originated from the noncentral asymmetric crystalline structure in piezoelectric materials is essential for PENGs to implement the conversion from mechanical energy to electrical energy. The harvested electricity is the prerequisite for subsequent demanded applications. Herein, we simply summarize two main types of mechanical energy for PENG to harvest: biomechanical activities and various mechanical energy from the natural environment (**Table 5**).

3.1. Energy Harvesting from Biomechanical Activities

According to the decrease in power dissipation of portable and biomedical electronics, harvesting micro/nanoenergy from

**ADVANCED
SCIENCE NEWS**
www.advancedsciencenews.com

**ADVANCED
FUNCTIONAL
MATERIALS**
www.afm-journal.de

Table 5. Different mechanical energy sources for energy harvesting.

		Energy sources	Voltage	Application
Biomechanical	Siddiqui et al.[166]	Human walking	25 V	Self-powered system
	Ye et al.[142]	Human motion	3.2–100 V	Power supply
	Kar et al.[167]	Human motion (finger tapping)	42 V	Power supply
	Ponnamma et al.[168]	Human motion (finger tapping, elbow movements)	6.5 V, 5.5 V	Wearable electronic textiles
	Dagdeviren et al.[169]	Bovine heart, lung diaphragm	4 V	Power supply
	Li et al.[170]	Porcine heart	17.5 V	Cardiac pacemaker
	Liu et al.[171]	Human motion (knee joint)	200 V	Cancer therapy
Natural environment	Yang et al.[172]	Highways	30–100 V	Wireless sensor networks
	Zhang et al.[173]	Road	Power density of 0.76 μW cm^{-3}	
	Garain et al.[174]	Wind	3 V	Self-powered sensor
	Du et al.[175]	Wind	2.81	
	Liu et al.[176]	Wind	25.8 V	Power supply
	Zhao et al.[177]	Wind	150 V	Power supply

their working/surrounding environments is a promising way to power these devices. As walking is the most common activity of human beings, it is convenient to integrate PEHs into shoes to convert the stepping energy into electricity. Siddiqui et al. demonstrated a nanofiber PENG for walking energy harvesting and realized the electrical energy storage in capacitors simultaneously.[166] As shown in **Figure 7**a, the device delivered an output of 25 V at a walking frequency of 0.6 Hz, displaying the ability to charge a 4.7 μF capacitor after about 72 steps to power sensors and had a good response to applied strains. Ye et al. found that foot stepping via a PENG with high performance and radiation shielding generated a high V_{OC} of 100 V, while the palm bending, elbow bending and finger taping delivered an output of 4.5, 4.5, and 15 V, respectively (Figure 7b).[142] Hu et al. developed a highly sensitive transparent PENG to harvest the energy from light tapping of a finger on a cell phone, achieving an output current of 0.8 nA.[178] The greatly improved electromechanical properties and the light transmittance of composite films were realized by aligned PZT nanowires in PDMS. They could also be used as antipeep films for cell phones. Kar et al. presented a facile but high-performance PENG at low cost, which could harvest mechanical energy from various motions, e.g., fingers imparting, body movements (heel, toe movement and wrist-twisting), speaking and air blowing.[167] With the achieved high power density of 4900 W m^{-3} and excellent piezoelectric energy conversion efficiency of 16.3%, the fabricated PENG could immediately light up 85 commercial LEDs by gently imparting on the PENG with fingers. Furthermore, the generated power could charge a 2.2 μF capacitor to 20 V within a few seconds by finger tapping on the PENG (Figure 7c). To get higher output performance, Ponnamma et al. designed a fiber mat-based PENG to harvest mechanical energy in different environments such as hand tapping and elbow movements.[168] After the PENG was attached to textile fabrics (Figure 7d), finger tapping collected a peak-to-peak V_{OC} of 6.5 V, and the elbow movements generated a 5.5 V of voltage. The above examples indicate that the PENG can achieve excellent output performance in many types of mechanical motions. It is closely related to the mechanical

properties, breakdown strength, and dielectric properties of piezoelectric films.

Energy harvesting and self-powered sensing strategies also provide practical and promising power and diagnosis solutions for implantable devices.[179–182] The self-sustainable energy harvesting can tremendously expand the lifetime and effectiveness of implantable biomedical devices. Wang et al. used P(VDF-TrFE) nanofibers by electrospinning to construct a PENG implanted subcutaneously in the thigh area of a rat, obtaining a V_{OC} of 6 mV and I_{SC} of 6 nA.[181] Dagdeviren et al. reported an integrated energy package to harvest the mechanical energy from the natural contractile and relaxation motions of the heart, lung, and diaphragm and store it to meet the practical powering requirements.[169] Lee and co-workers demonstrated self-powered wireless data transmission based on a high-performance PENG by harvesting biomechanical energy in a large animal model.[183] The energy harvester collected a 17.8 V of voltage and 1.75 μA of current from the contraction and relaxation of a porcine heart, showing a great improvement by 17.5 times as compared with Dagdeviren's demonstration. Afterward, another typical research work reported an integration strategy for directly powering a cardiac pacemaker,[170] which obtained a significantly improved I_{SC} of 15 μA over state-of-the-art performance via harvesting energy from the kinetic heartbeat in vivo (Figure 7e). It achieved impressive progress in the fabrication of a self-powered or batteryless cardiac pacemaker. Kondapalli et al. also demonstrated a small PENG placed on valvular regions of the heart to collect energy from cardiac valvular perturbations and power a wireless sonomicrometry sensor.[184]

More importantly, the harvested biomechanical energy can also be applied to bioelectronic devices for medical treatment in addition to a self-powered system.[185] Liu et al. reported a self-powered photodynamic system (s-PDT) for long-term autonomous cancer therapy powered by human motions.[171] The s-PDT system is shown in Figure 7f-I, which included a twinning structured PENG as an energy-harvesting unit, energy management unit (PMU), μ-LED, and photosensitizer. As an energy harvester, it can convert biomechanical energy from joint motion into electrical energy, which serves as a power

**ADVANCED
SCIENCE NEWS**

www.advancedsciencenews.com

**ADVANCED
FUNCTIONAL
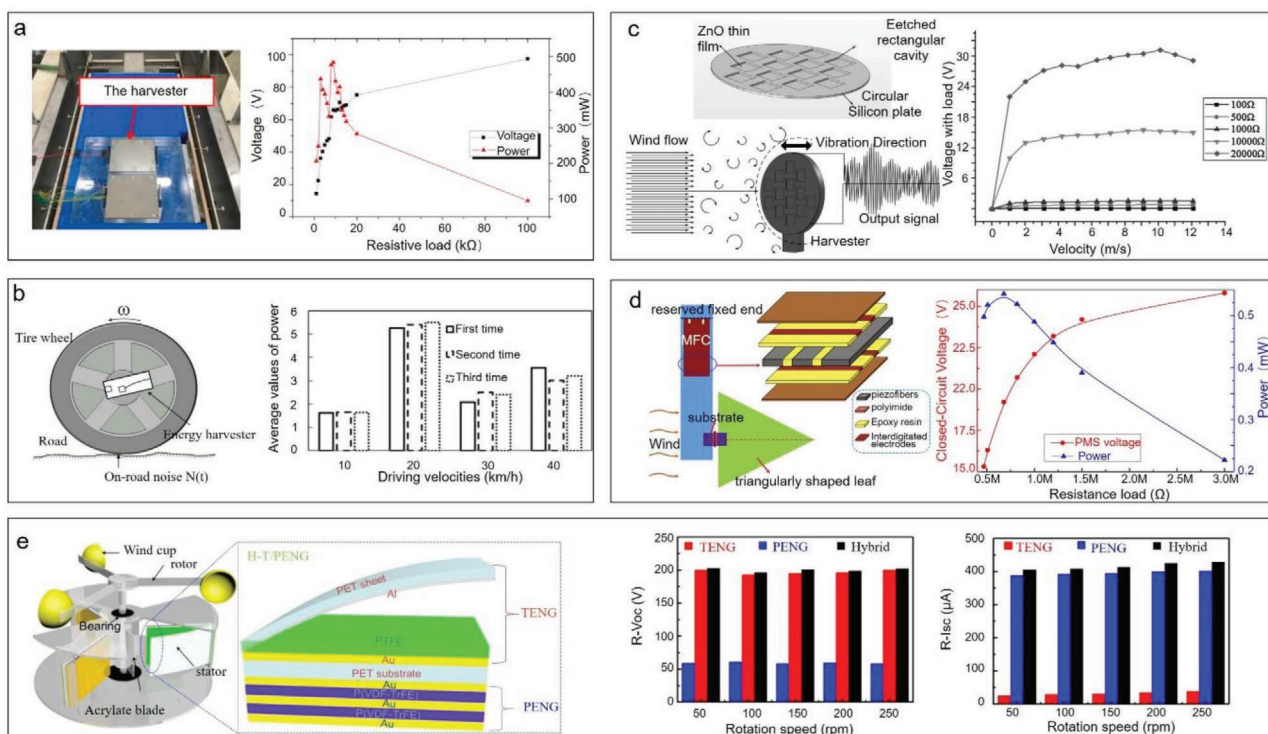MATERIALS**

www.afm-journal.de
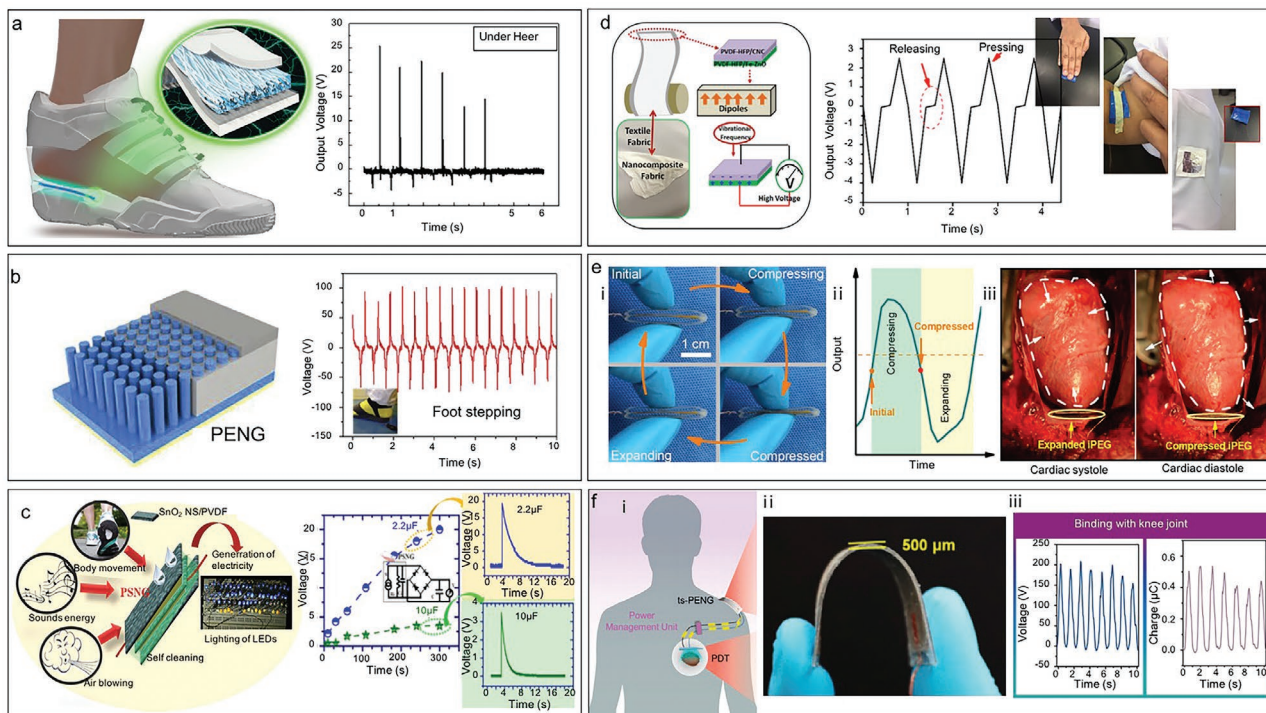
Figure 7. a) Schematic of inserting nanofiber PENGs into shoes, the highlighted area shows the device position, and open-circuit voltage of nf-PENG during human walking when placed inside of the shoe under the heel. Reproduced with permission.[166] Copyright 2016, Elsevier Ltd. b) The schematic diagram of piezoelectric nanogenerator structure and output voltage generated from flexible PENGs by foot stepping. Reproduced with permission.[142] Copyright 2019, Elsevier Ltd. c) Schematic application of the PSNG, charging of the capacitors (2.2 and 10 μF) generated from the PSNG under periodic finger imparting process using a full wave rectifier, and the pointed figure shows discharging of the capacitor recorded through the digital storage oscilloscope. Reproduced with permission.[167] Copyright 2019, Elsevier Ltd. d) Schematic for the piezoelectric nanogenerator design and output voltage of the PENG with hand tapping; insets show energy harvest from elbow movement and shoulder movement. Reproduced with permission.[168] Copyright 2019, The Authors. Published by Elsevier Ltd. e) Photograph of the piezoelectric composite bent by human fingers. I) Shape changes and II) the corresponding output of the iPENG in one working circle. III) Photographs of the iPENG in the pericardial sac fixed at AP, showing that the iPENG expands during cardiac systolic phase (left) and then is compressed by the heart during cardiac diastolic phase (right). Reproduced with permission.[170] Copyright 2019, American Chemical Society. f-I) s-PDT system consisting of ts-PENG, PMU, m-LED, and a photosensitizer. II) Photograph of the ts-PENG in the bending state. III) V_{OC} and Q_{SC} of the ts-PENG binding with the knee joint. Reproduced with permission.[171] Copyright 2020, American Chemical Society.

source to drive the PDT system. As shown in Figure 7f-II, the twinning structured PENG generated a V_{OC} of 200 V and a Q_{SC} of 0.5 μC by bending the knee joint. The s-PDT had two different work modes, which could be managed independently by patients. When the μ-LED was implanted subcutaneously in mice with transplanted tumors, the s-PDT system presented an obvious antitumor effect through intermittent continuous light stimulation mode for 12 days, achieving a tumor inhibition rate at 87.46%. This novel s-PDT system combined with two treatment modes may offer a great opportunity to develop wearable/implantable and energy-autonomy devices for long-term photodynamic therapy, which will be a prospective and effective method for clinical treatment of cancer.

3.2. Energy Harvesting from the Natural Environment

The ambient environments of human beings offer various occasions for mechanical energy harvesting, e.g., railway/highway/crosswalk, machine vibration, wind energy, blue energy, etc. Energy-harvesting technologies in different types

of applications (or occasions) have been studied for years, such as the railway, car tire, and pavement. The ambient environments of roads (or bridges) are rich in human activities and mechanical energy in surroundings, which exhibit great potential and strong practicality for energy harvesting. For example, Yang et al. developed the PEHs on the road to collect the force energy and serve as a power supply for wireless sensor networks in smart highways (**Figure 8**a).[172] This device had a high output power of 483 mW (power density of 21.47 W m^{-2}), which was greatly larger than that of the existing PEHs. In the case of wheel rotation, an energy harvester was demonstrated to be installed on the front tire wheel and generate an average power of 0.0052 mW at the speed of 20 km h^{-1} (Figure 8b). The energy-harvesting performance was comprehensively investigated by Zhang et al. through both simulation and laboratory experimental analyses.[173] In another work of them, piezoelectric bistable structures were used to collect the mechanical energy from rotational tires, and the maximum power generation reached 0.24 mW at the speed of 40 km h^{-1}.[186] Hu et al. integrated PENG on the inner surface of the tire to harvest mechanical energy originated from the tire deformation during

**ADVANCED
SCIENCE NEWS**

www.advancedsciencenews.com

**ADVANCED
FUNCTIONAL
MATERIALS**

www.afm-journal.de

Figure 8. a) Experimental setup of the road energy harvester, voltage, and power from the device. Reproduced with permission.[172] Copyright 2017, Elsevier B.V. b) Illustration of the energy harvester attached to the center of a wheel and average values of the collected power under four different speeds. Reproduced with permission.[173] Copyright 2016 by the authors. c) The diagram principle of the energy harvester and load voltage of device in different wind velocities. Reproduced with permission.[175] Copyright 2017, Elsevier B.V. d) Schematic diagram of PEH structure and the cross-sectional layout of the MFC, closed-circuit voltage (red line), and power harvest (blue line) for PEH–MFC connecting with various resistance loads. Reproduced with permission.[176] Copyright 2020, Elsevier B.V. e) Schematic illustration of the H-P/TENGs mounted in the custom frame. Inset is the enlarged structure of single H-P/TENG, the rectified open-circuit voltage, and short-circuit current of TENG, PENG, and H-P/TENG at rotation speeds from 50 to 250 rpm. Reproduced with permission.[177] Copyright 2018, Elsevier Ltd.

the car-driving process.[187] The measured output voltage and current of the PENG under these conditions were 1.5 V and 25 nA, respectively, and the maximum output power density was 70 µW cm^{-3}. Thus, it could directly light an LCD screen.

Wind energy is also an ideal and environmentally friendly source for microenergy-harvesting based on PENGs. Du et al. reported a wind energy harvester based on a circular silicon plate with several patterned and symmetrically distributed rectangular cavities covered with ZnO thin films (Figure 8c).[175] It was prepared by a microelectromechanical system (MEMS). Its maximum output power density reached 23.39 nW cm^{-2}. The device worked well when the wind blew from only one direction, which was generally not the case in the natural environment (the wind direction usually changed over time). Zhao et al. demonstrated an arc-shaped PENG capable of harvesting the energy through the wind coming from different directions with a wide speed range (2–17 m s^{-1}).[188] When the connected external load was 15 kΩ, the PENG showed a peak output power of 1.73 mW at 17 m s^{-1}. To better power electronic devices, Orrego et al. developed an inverted flag-shaped PENG to harvest ambient wind energy, which exhibited a peak electrical power of 5.0 mW cm^{-3} at a wind velocity of 9 m s^{-1}.[189] They also confirmed that the inverted flag-shaped PENG could be operated in an ambient environment under fluctuant wind conditions (both magnitude and direction). The collected wind

energy successfully powered a temperature sensor. Notably, for wind energy harvesting, the vibration mode is one of the most important factors that influence the energy conversion efficiency. Liu et al. designed a PEH in the highly efficient flutter mode by taking advantage of flexible macrofiber composites, as well as the highly efficient flutter mode (Figure 8d).[176] With a load resistance of 680 kΩ, the resulting direct voltage and electric power were obtained to be 25.8 V and 0.54 mW, respectively. It was concluded that the proposed energy harvesting system based on the macrofiber composite under the flutter mode could obtain an output power density of 9.18 mW cm^{-3}, meeting the requirement of conventional MEMS. The hybridization of various NGs offered an efficient method to strengthening the output power via simultaneously harvesting different types of energy.[190,191] Zhao et al. integrated the bimorph-based PENG into a triboelectric nanogenerator to fabricate a hybrid piezo/triboelectric nanogenerator (H-P/TENG) for highly efficient mechanical rotation of energy harvesting.[177] The PENG showed high output current and low output voltage, which was appropriately complementary with the TENG output performance. As shown in Figure 8e, the maximum V_{OC} and I_{SC} of H-P/TENG are 200 V and 400 µA with a rotation speed at 100 rpm. The H-P/TENG inherited the merits of both types of NGs (i.e., high output voltage and current) and presented great potential for energy harvesting from surroundings for

Table 6. Comparison of different PENGs for various sensors.

	Voltage	Sensitivity	Application
Guo et al.[192]	10 V	$\Delta R/R \approx 670\%$	NO_2 gas sensor
Fu et al.[193]	30 mV	0.28 mV deg^{-1}	Strain sensor
Deng et al.[16]	11.5 V	0.33 V kPa^{-1}	Strain sensor
Zhang et al.[194]	250 mV	2.476 mV s mm^{-1}	Hydrodynamic sensor
Ahn et al.[195]	4.6 V	0.18 V kPa^{-1}	Strain sensor
Zhao et al.[196]	5 V	8.85 nA K^{-1}	Temperature sensor
		0.42 nA cm^2 mW^{-1}	Light sensor
		1.43 nA kPa^{-1}	Pressure sensor

the self-powered systems. At the wind speed of 14 m s^{-1}, high output voltage of 150 V and current of 150 µA could be used for powering 50 LEDs.

4. Applications in Self-Powered Active Sensors

A self-powered system based on nanogenerator technology is highly desirable for low power electronics, the Internet of Things, human–machine interaction, wearable electronic devices, and implanted biomedical devices. In this aspect, PENGs, which are preferential for the utilization of harvested mechanical energy (or piezoelectric effect) to drive various sensors (or enhance sensing performance), have gained more significant attentions ranging from strain sensors, gas sensors, humidity sensors, pressure sensors, and biosensors. Based on the enhanced piezoelectric output during the last decades, lots of sophisticated self-powered sensing applications based on PENGs have been reported. In the following sections, we divided the PENG-based active functional sensors into four categories, covering human motion monitoring, biomedical applications, environment monitoring, and artificial intelligence (**Table 6**).

4.1. Active Sensors for Human Motion Monitoring

With the development of emerging soft electronics, flexible sensors and sensory systems can be integrated into the human body or skin (by sticking-on or wearable solutions). These approaches have been extensively applied to human motion monitoring (e.g., eyeball motion, joint motion, gesture monitor, etc.), which are significant in the fields of sports training or fitness management. **Figure 9**a shows that different
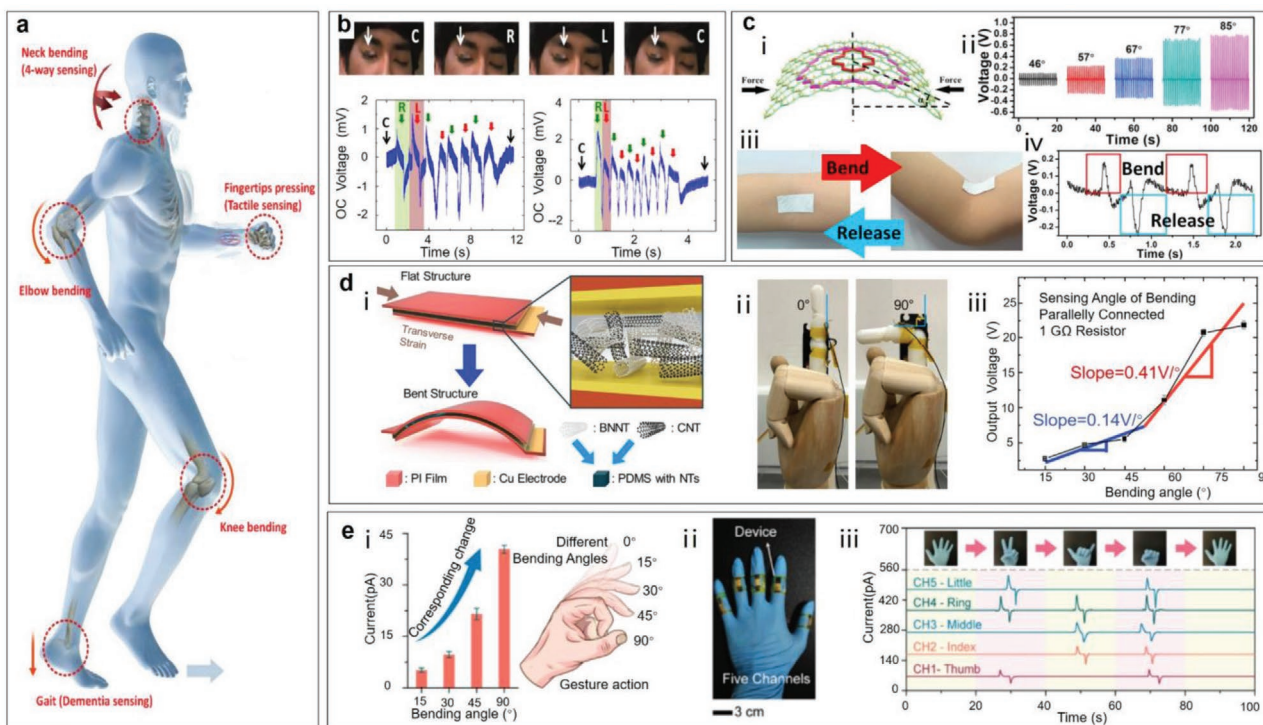
Figure 9. a) Schematic illustration of wearable self-powered sensor applied to body. Reproduced with permission.[195] Copyright 2020, Elsevier Ltd. b) The NG attached to a right eyelid was driven by moving the eye ball from right (R), center (C), and to left (L) or from L, C, and R. Output voltage measured under slow and rapid eye movement. Reproduced with permission.[197] Copyright 2013, Wiley-VCH GmbH. c-I) Schematic illustration showing the bending deformation of the e-skin. II) The outputting piezoelectric voltage of the e-skin under different bending angles. III) Picture and IV) output voltage of elbow bending and releasing by the e-skin. Reproduced with permission.[199] Copyright 2016, Elsevier Ltd. d-I) Flat structure, bent structure, and the schematic illustration of the inside of the composite layer. II) Finger models without bending and with 90° bending. III) Kinematic sensor response with sensitivity. Reproduced with permission.[200] Copyright 2020, American Chemical Society. e-I) Schematic diagram of gesture action and the output property of the device. II) Photograph of the devices bound to five fingers. III) Multiple gestures with a multichannel system and its short-circuit current power. Reproduced with permission.[202] Copyright 2020, Elsevier Ltd.

ADVANCED
SCIENCE NEWS
www.advancedsciencenews.com

ADVANCED
FUNCTIONAL
**MATERIALS**
www.afm-journal.de

positions of the human body can be applied with relevant active sensors. The motion of the body has relatively large displacement and thereby is relatively easy for PENGs to detect. The PENG-based self-powered human motion sensors can detect not only qualitative but also quantitative information of the motion. For instance, Lee et al. reported an ultrathin PENG with a total thickness of 16 µm as an active sensor for monitoring local deformation.[197] The superflexible nanogenerator showed great potential to work as an active strain sensor, which could be attached to the eyelid surface and used to detect the movement of the eyeball to monitor sleep patterns, fatigue, and possible brain activity (Figure 9b). Chun et al. fabricated NGs based on the highly stretchable piezoelectric composite as a self-powered ultrasensitive sensor for providing direction information on the wrist motions.[198] He et al. developed a multifunctional flexible self-powered ZnO/PVDF/fabric e-skin.[199] The piezoelectric effect of ZnO/PVDF led to motion-powered tactile-perception behaviors, which could detect elbow bending and finger pressing (Figure 9c). Kim et al. fabricated a contact-electrification-assisted PENG based on BNNTs and CNTs.[200] It consisted of two electrode layers and a mechanically robust BNNT–CNT–PDMS composite layer (Figure 9d-i). They obtained optimum conditions of the highest electrical output by changing the measurement conditions of moving distances, bending displacements, poling parameters, and humidity environment. Moreover, the bending angles of the finger were successfully detected by the attached PENG, which exhibited a sensitivity of 0.14 V deg^{-1} from 15° to 45° and 0.47 V deg^{-1} from 60° to 90°, respectively (Figure 9d-ii,iii). Yang et al. prepared a piezoelectric composite film consisting of BaTiO$_3$ modified by polydopamine and PVDF for pressure sensors,[201] which exhibited a remarkable piezoelectric V_{OC} of 9.3 V and a fast response of 61 ms. The sensor was used to detect joint bending and human motions, showing distinguish signal curves. Huo et al. synthesized the Sb-doped ZnO NW films with variable aspect-ratio via the low-temperature hydrothermal method and studied their piezoelectric effect to fabricate a flexible self-powered strain sensor.[202] This sensor was used to detect strain information and monitor diverse gestures motion. Figure 9e-i shows that the output current was proportionally correlated with the bending degree of fingers. A multichannel data acquisition system was used to simulate the electrical signals driven by multiple motions to display gesture movements (Figure 9e-iii). The devices discussed above were light in weight, easy to prepare and low in cost, which provided effective routes to the applications of flexible electronic devices, wearable devices, and robotics. Apart from this, active matrix networks based on transistors and integrated with piezoelectric materials could provide advanced sensing performance, such as low signal crosstalk, multiparameter monitoring, high sensitivity, and high spatial resolution. Sun et al. combined PENGs with planar graphene transistors to develop a piezoelectric potential active-matrix strain sensor array.[203] The piezoelectric potential was effectively coupled to the graphene channel through the ion gel dielectrics, which also induced corresponding sensing signals according to the applied different strains. The strain sensor displayed excellent sensitivity (gauge factor at 389), a minimum detectable strain of as low as 0.008% and high mechanical durability. They fabricated transparent and stretchable strain sensors

to monitor human hand movement, representing a significant advance in a more general field of piezotronic sensing array.

4.2. Active Sensors for Biomedical Applications

Real-time monitoring of human physiological signals (e.g., carotid artery and wrist pulsation, vocal cord vibration, muscle behavior, etc.) are of great significance for disease diagnosis, therapy, rehabilitation, and health assessment.[193,204–207] The flexible piezoelectric sensors have outstanding advantages of fast response and self-powered characteristics, providing extensive promise for biomedical fields in wearable electronics.[208] In recent years, a large number of PENG-based biosensors have been reported for physiological signal monitoring. **Figure 10**a summarizes the reported examples of physiological signal monitoring in different parts of human body.[62,209] Fu et al. developed a self-powered hydrogel based on polyacrylonitrile–poly(vinylidene fluoride), which showed a good stretchability of 175% and high toughness of 1.23 MJ m^{-2}.[193] As shown in Figure 10, the hydrogel-based skin sensor is attached to the wrist and throat to monitor body pulse signal and spoken words, respectively. Chen et al. fabricated a highly sensitive self-powered PENG sensor based on nanocomposite micropillar array to work in a noncontact mode for detecting air pressure/flow.[210] It can also be used to measure human breathing. Xue et al. integrated the PVDF NG on a respirator to work as a self-powered sensor for monitoring human breathing.[211] Meantime, it can also be used to monitor ambient temperature due to the pyroelectric characteristics of PVDF film. Park et al. demonstrated a self-powered ultrathin piezoelectric pulse sensor based on PZT thin film, which was conformally attached to the human epidermis to detect the radial/carotid artery pulse, respiratory activities, and trachea movements.[212] Moreover, the pulse signal was transmitted to the smartphone wirelessly via a microcontroller unit and Bluetooth transmitter, realizing the self-powered real-time pulse monitoring system. Yang et al. fabricated a piezoelectric sensor constructed from 3D layered PVDF/ZnO nanofibers, based on which the achieved physiological monitoring system was of good flexibility, outstanding mechanical stability and high gas permeability.[62] Figure 10c-I shows the V_{OC} of the device according to different curvatures, revealing a linear correlation. Therefore, the 3D PVDF/ZnO nanofiber-based piezoelectric sensor was successfully developed for human physiological monitoring such as respiration, heart rate, and gait recognition. As shown in Figure 10c-II, the detected breathing signal during attaching the piezoelectric sensor to the chest could completely match with the actual breathing cycle. These results verified that the piezoelectric sensors were capable to clearly differentiate breathing modes among normal breathing, deep breathing, and gasping. When the piezoelectric sensor is conformally mounted on the wrist, it can clearly indicate the pulse signals, thus assisting in relevant clinical applications (Figure 10c-III), such as detection of hypertension, diagnosis, and prevention of cardiovascular disease. Furthermore, it can be attached to the epidermis of the calf muscle for gait recognition (Figure 10c-IV).

Implantable electronic devices have also been showed significant advantages in continuous and real-time monitoring
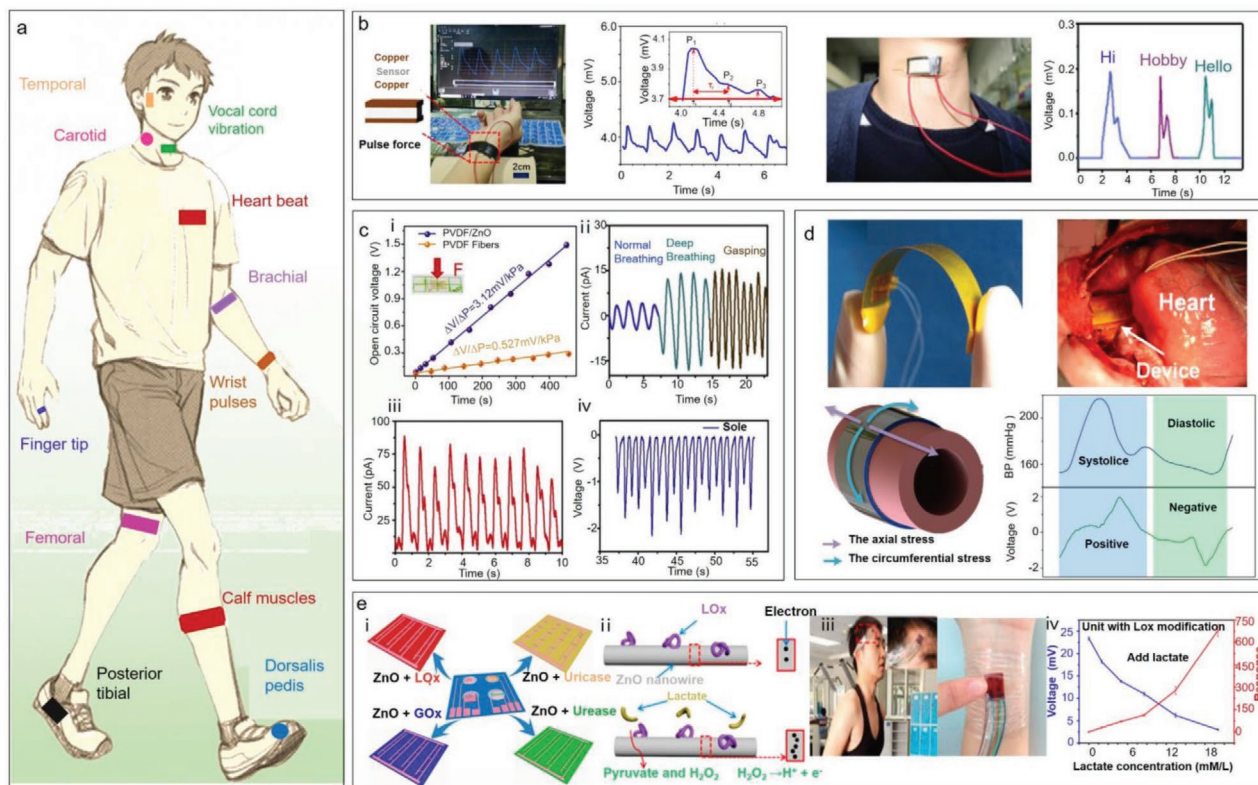
Figure 10. a) Schematic illustration of recent researches on the physiological monitoring of the arterial pulse sites and vibration. Adapted with permission.[62] Copyright 2020, Elsevier Ltd. Reproduced with permission.[209] Copyright 2019, Wiley-VCH GmbH. b) Photograph and model illustration of a wearable pulse monitor to measure radial artery and the pulse waveform, the optical photo vocal cord vibration detection, and voltage signal output diagrams for speaking different words (hi, hobby, and hello, respectively). Reproduced with permission.[93] Copyright 2019, American Chemical Society. c) Dependence of the open-circuit voltage of the device with pressure, the electrical outputs of different breathing patterns, the real-time signals of wrist pulses, and multiple signals of the left leg when walking left. Reproduced with permission.[62] Copyright 2020, Elsevier Ltd. d) Photograph of the device showing its flexibility and the device wrapping on the ascending aorta of porcine, the circumferential stress in expanded aorta wall and the distribution of induced charge in device, and waveform comparison of the BP with output voltage of the device. Reproduced with permission.[214] Copyright 2016, Elsevier Ltd. e) Schematic diagram of four piezobiosensing units, working mechanism of electronic-skin for perspiration analysis, the electronic-skin attached on the forehead and wrist, and the voltage and response against different lactate concentrations. Reproduced with permission.[215] Copyright 2017, American Chemical Society.

or medical treatment in vivo during the past two decades.[213] PENG-based implantable self-powered devices can solve the problem of the limited battery life of traditional devices. Cheng et al. reported an implantable and self-powered sensor based on the piezoelectric thin film for blood pressure monitoring in vivo (Figure 10d).[214] A good linear relationship between the output voltage and blood pressure via both in vitro and in vivo studies is promising for an implantable, self-powered, and visualized blood pressure monitoring system. A hypertension status can be visually alarmed in real-time through this battery-free system.

Furthermore, some flexible biosensors can also be used to detect personal physiological metabolic indicators, such as lactate, glucose, blood glucose, electrolyte balance, and so on. In human sweat, biomolecules and inorganic salts have various physiological information, so that it could achieve the noninvasively and real-time monitor of human body through the analysis of the composition of sweat. Han et al. proposed a self-powered wearable noninvasive electronic skin for sweat analysis.[215] Figure 10e-I shows the piezobiosensing unit of

enzyme/ZnO arrays. The enzymes modified on the surface of ZnO nanowires include lactate oxidase (LOx), glucose oxidase (GOx), uricase, and urease. The electronic skin could detect lactate, glucose, uric acid, and urea in the perspiration through the active piezoelectric signal. Figure 10e-II schematically illustrates the detailed working mechanism of the LO_x piezobiosensing unit. When it is immersed in the lactate aqueous solution, the enzymatic reaction takes place and the surface carrier density will increase, which results in the decreased piezoelectric voltage due to the strong piezoscreening effect. Then, the response of the piezobiosensing unit as a function of the lactate concentration can be obtained (Figure 10e-IV). The piezobiosensing unit can be attached to the forehead or wrist to continuously monitor the physiological state in real time. They also fabricated a self-powered implantable skin-like glucometer for real-time detection of blood glucose level in vivo.[216] When the skin-like glucometer was implanted into the mouse body, the device ran well in the live mouse and detected the glucose level in real time.

**ADVANCED
SCIENCE NEWS**

www.advancedsciencenews.com

**ADVANCED
FUNCTIONAL
MATERIALS**

www.afm-journal.de

4.3. Active Sensors for Environment Monitoring

With the fast development of industry and the acceleration of urbanization, the scale of pollution emissions has also expanded dramatically. During the past decades, gas sensing techniques have attracted worldwide attention, in which the semiconducting metal oxide NWs have strengthened the sensitivity and stability among the resistant-type gas sensors owing to their high surface volume ratio. For example, previous reports have demonstrated that ZnO nanostructure-based gas sensors exhibit a good response to many toxic gases (such as triethylamine,[217] SO_2,[218] H_2S,[219] CO, and NH_3[220]) and moisture air.[122] These nanoscale gas sensors are small in size, but the generally required large electric power source limits their application as portable or wearable systems. Self-powered sensors that can collect energy from the ambient environment and use it to power themselves have become one of the attractive studies in the field of gas monitoring. Xue's group demonstrated a new type H_2S gas sensor via combining the piezoelectric and gas sensing properties of ZnO NWs. The piezoelectric output of ZnO nanogenerator acted as both the power supply and H_2S sensing signal to detect H_2S without external power source.[221] Subsequently, they achieved higher-performance piezo-H_2S sensors by introducing heterostructures, such as CuO/ZnO,[222] In_2O_3/ZnO,[223] and NiO/ZnO.[163] As shown in **Figure 11**a, they developed NiO/ZnO NWs in different composition ratios as self-powered piezo-H_2S sensors with high sensitivity and fast response. Adsorption of gas molecules on the surface of ZnO NWs led to the increase of free carrier density in ZnO and corresponding output. When the external strain was applied to the gas sensor, the piezoelectric output was reduced due to the screening effect of piezopotential induced charges. When the sensor was exposed to 1000 ppm H_2S at room

temperature, the response of NiO/ZnO NW (0.5 м composition ratio) was 536 and the sensitivity was 0.49. The high sensitivity can be attributed to the coupling effect of the construction of NiO/ZnO PN-junction sensing and piezoelectric screening effect (enhance the output variations). They also reported a high-performance humidity sensor based on the Fe-doped ZnO nanoarrays.[122] The doping of Fe led to a high charge density, so that the piezoelectric screening effect was easier to decrease the output when the water molecules were adsorbed on the surface of Fe-doped ZnO NWs. Figure 11b shows the response of undoped, 0.5%, 1%, and 2% Fe-doped ZnO NW arrays at different levels of relative humidity. These results show that 1% Fe-doped ZnO NW arrays exhibit the largest response and have potential applications in self-powered/active humidity sensors.

Recent research reported that $BiFeO_3$ nanoparticles can also be applied to self-powered sensors. K S et al. proposed a highly reliable transitional-flow-based PENG in hollow-tube shape (made of the $BiFeO_3$), which could work as a self-powered catechol sensor (SPCS) to detect the organic contaminants in water samples.[224] As shown in Figure 11c, when a fluid flows through the hollow-tube-shaped PENG, there is a corresponding output voltage response due to the synergistic effect of the liquid flow pressure and the chemical adsorption reaction of catechol solution and $BiFeO_3$ nanoparticles through the interactions hole. Hollow-tube-shaped $BiFeO_3$ PENG has a V_{OC} of 223 V and an output power of 2.624 mW m^{-2} at 1 Hz frequency. It can work as a micropower supply as well as an active biosensor, showing high selectivity and excellent detection limit down to 10.2×10^{-6} м.

Researchers had also attempted to develop hydrodynamic sensing systems based on the piezoelectric effect for autonomous underwater vehicles, so as to perceive their surroundings for navigation and obstacle avoidance.[225] Inspired by the universal lateral-line system of fish, Zhang et al. designed
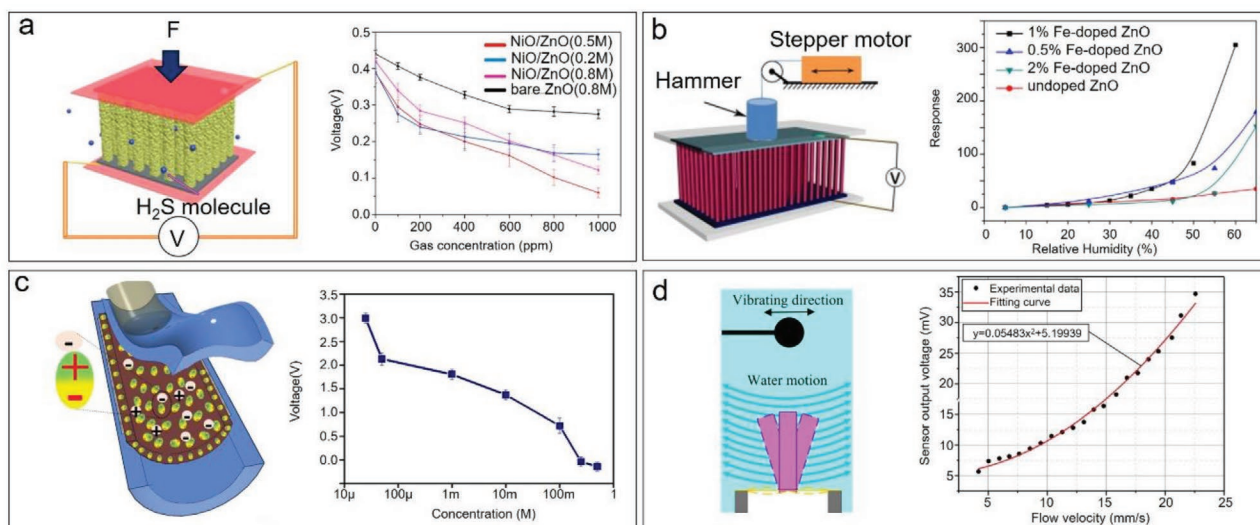
Figure 11. a) The schematic mechanism of device structure and the piezovoltage of bare ZnO NWs and NiO/ZnO (0.2, 0.5, and 0.8 м) NWs in different concentrations of H_2S at room temperature. Reproduced with permission.[163] Copyright 2015, Elsevier B.V. b) The measurement of the piezoelectric output voltage and the response of undoped, 0.5%, 1%, and 2% Fe-doped ZnO NW arrays at different relative humidities. Reproduced with permission.[122] Copyright 2015, Elsevier B.V. c) The schematic mechanism of the device with 50×10^{-6} м catechol solution and the output voltage response of the TFPNG-SPCS device during the pulsed catechol fluid flow as a function of different solution concentrations. Reproduced with permission.[224] Copyright 2020, Elsevier B.V. d) Schematic of the sensing principle and experimental results of the oscillatory water flow velocity sensing. Reproduced with permission.[194] Copyright 2019, Elsevier Ltd.

a liquid flow sensor inspired by the lateral-line system of fish consisting of a radial field piezoelectric diaphragm and a high aspect ratio 3D-printed pillar.[194] Figure 11d shows the schematic of the relevant sensing principle. When a sphere vibrates in water, the generated oscillating flow will act as a stimulus, eventually causing stress on the diaphragm of the designed sensor and resulting in an output voltage. A linear relationship was found between oscillating water flow velocity and pressure, together with a high sensitivity of 2.476 mV s mm^{-1} at 35 Hz hydrodynamic flows and a good response to the low-frequency underwater disturbances phenomena.

4.4. Active Sensors for Artificial Intelligence

As artificial intelligence develops rapidly, an increasing number of intelligent devices have been developed.[226–228] To power

intelligent devices, a large number of sensing nodes are required in the sensory network. Currently, commercial batteries universally used usually have limited lifecycles and are harmful to the environment, which hinder more practical applications in IoTs. Therefore, self-powered piezoelectric sensors without any requirement for batteries are superior candidates in wireless sensor networks.[229] With the increasingly developed devices for energy harvesting and power management electronics, self-powered wireless intelligent systems aiming at standalone, mobile, and ubiquitous sensory networks have become a research hotspot for intelligent applications.[230]

Examples of active sensors for intelligent remote control are shown in **Figure 12**. Based on the cowpea-structured PVDF/ZnO nanofibers, Deng et al. proposed a self-powered flexible piezoelectric sensor to recognize gestures, so as to realize remote control in a human–machine interactive (HMI) system.[12] Owing to the excellent flexibility of polymer and
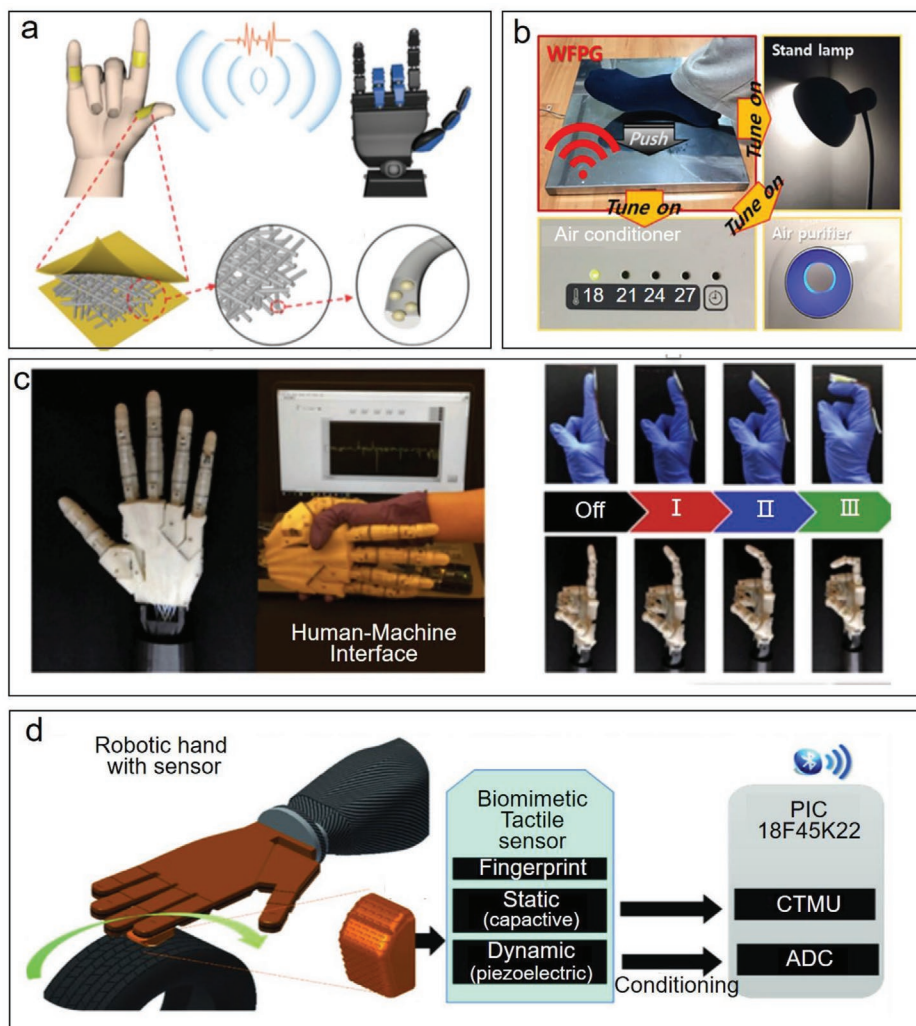
Figure 12. Active sensors for intelligent remote control. a) The schematic diagram of the developed smart sensor applied in the field of intelligent human–machine interface. Reproduced with permission.[12] Copyright 2018, Elsevier Ltd. b) A wireless sensor system for smart home, which can control an air conditioner, a table lamp, and an air purifier. Reproduced with permission.[231] Copyright 2018, Elsevier Ltd. c) The human–robot imitation is demonstrated by the smart sign sensor. Reproduced with permission.[232] Copyright 2020, Elsevier Ltd. d) The fingerprint-enhanced biomimetic sensor and its application of wireless communication via Bluetooth. Reproduced with permission.[233] Copyright 2019, The Authors. Published by Wiley-VCH GmbH.

ADVANCED
SCIENCE NEWS
www.advancedsciencenews.com

ADVANCED
FUNCTIONAL
MATERIALS
www.afm-journal.de

the synergistic piezoelectric effect of hybrid PVDF/ZnO, the piezosensor not only exhibited superior bending sensitivity of 4.4 mV deg^{-1} vary from 44° to 122°, but also responded quickly in 76 ms. When the piezosensor was integrated into an intelligent human–machine interface, it was conformably covered on different curved-surfaces to accurately record the bending angles and realize fast recognition, exhibiting big advantages in intelligent human–machine interaction. Thus, the robotic hand for remote control was demonstrated by synchronously doing the same gesture with the human hand attached to the piezosensor (Figure 12a). These results provided great potential for physical signal monitoring, gesture sensing, and some interesting applications in intelligent HMI.

Kim et al. designed an innovative piezoelectric material (optimized PZN0.25C ceramics) to fabricate smart-home sensors that could be attached to the floor tile.[231] When stepping on the floor, a peak V_{OC} of 42 V and a current of 11 µA were generated resulting from the piezoelectric effect (Figure 12b). Once the signals were detected, real-time powering-on/off and control over home appliances could be conducted through a microcontroller unit. Yang et al. demonstrated a 2D SnS$_2$-based PENG device to investigate the simultaneously human–robot control in an intelligent HMI system.[232] As shown in Figure 12c, the distinctive voltages can be generated by human forefingers in various bending states (off, I, II, and III). The distinctive voltages were then used to achieve simultaneous human–robot control with the same bending states, which realized the real-time human–robot control to imitate human gestures. This work demonstrated 2D material-based devices toward multifunctional biomechanical harvesters, opening up an important research direction toward active-sensing technology and HMI.

Navaraj and Dahiya demonstrated a dynamic piezoelectric tactile sensor. It is interfaced with a metal oxide semiconductor field-effect transistor (MOSFET) through an extended gate and a common source configuration, exhibiting a sensitivity of 2.28 kPa^{-1}.[233] Through the closed-loop tactile scan ultilizing an intelligent robotic arm, the captured tactile signals (as latency-code spikes) were fed into a spiking neural network (SNN) tempotron classifier system to train the SNN model. A classification accuracy of 99.45% was achieved to enable a real-time binary texture classification, exhibiting great potential in prosthesis, robotics, medical devices, and wearable sensors (Figure 12d).
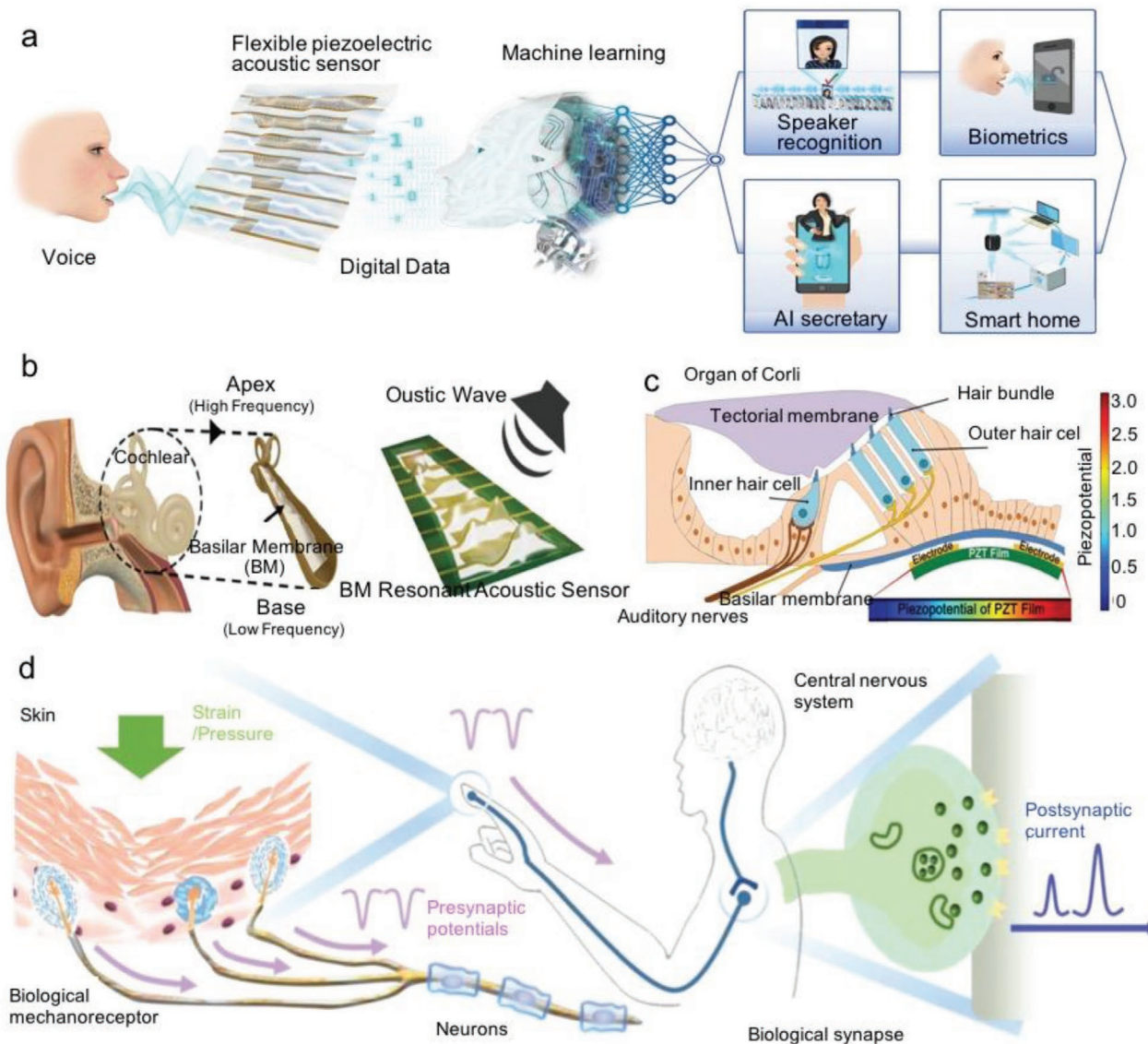
Regarding the artificial intelligence applications of piezoelectric sensors, flexible acoustic sensors for speech recognition and artificial synapses have been spotlighted as well. Piezoelectric acoustic sensors with excellent inherent piezoelectric properties promise as an excellent candidate to improve sensitivity and speech recognition accuracy.[234–236] As illustrated in **Figure 13**a, the speech recognition system generally includes two indispensable parts: i) acoustic hardware sensors; ii) speech recognition software. The sound pressure of human utterance is perceived by the acoustic sensors.[237] Through the acoustic hardware sensors, the original speech sound is converted into analog electrical data.[238–242] The piezoelectric acoustic sensor can covert utterance into various analog electrical signals via vibrating in the wake of the speaker's voice, thus providing large amounts of data for prepocessing and model training. The data is then trained based on a machine learning model and to extract the voice features.[243–245]

Han et al. reported a self-powered flexible piezoelectric acoustic sensor (f-PAS) inspired by the basilar membrane in human cochlear.[246] The acoustic sensor based on the PZT membrane produced abundant distinct voltages by the multiple vibration of the piezoelectric membrane sensor in response to the minute acoustic sound stimuli (Figure 13b). Through the combination of multiresonant frequency tuning and low-quality factor (Q), the sensing range of f-PAS is able to cover the voice frequency spectrum. The f-PAS exhibited a sensitivity eight times larger than the conventional acoustic sensor. Lee et al. proposed a novel inorganic-based piezoelectric acoustic nanosensor (iPANS) based on PZT thin film to imutate the biofunctions of the natural basilar membrane (BM).[247] Figure 13c shows the conceptual schematics of organ of Corti in mammalian cochlea and describes the PZT thin film beneath the BM with response to the acoustic sound stimuli. During the experiment, the trapezoidal silicone-based membrane (SM) was selected to imutate the biofunctions of the original human hair cells for frequency selectivity. To get over the brittle problem of inorganic piezoelectric materials, a flexible iPANS was fabricated on the SM via laser lift-off technology. The piezoelectric sensing signals and the vibration amplitude were detected and analyzed by the finite element analysis under experimental conditions. A highly efficient sensitivity was achieve by the iPANS. Furthermore, the electrical output in the small motion state (≈15 nm) of SM can response to the speech stimuli in the audible frequency range.

The human somatosensory system composed of biological stimuli receptors, transmission neurons, and synapses is an intermediary for sensing external biomechanical stimulation and signal transmission/processing (Figure 13d). The artificial synaptic devices have been extensively reported in previous studies.[248–257] Further developing sophisticated artificial sensory synapses is of great significance to neuromorphic interface of neurorobots, future self-powered electronic skin, human–computer interaction, artificial intelligence, etc.[258,259] Sun's group developed a piezoelectric graphene artificial sensory synapse by coupling PENG with an electrical double layer transistor.[260] Piezoelectric potential from PENG could effectively power the synaptic device. Piezoelectric artificial synapses used external strains, ions in ion gel dielectrics, and graphene channel current to simulate sensory/presynaptic input, neurotransmitter, and postsynaptic output terminals in biological sensory synapses. It realized the external stimulus/perception and synaptic transmission in the proposed neuromorphic system. In another work, they also used PENG to develop a mechanically programmed nonvolatile memory array based on the piezopotential powered oxide transistor.[261] Compared with traditional memory devices, it presented lower power consumption and realized the programming/erasing process through mechanical behaviors. It could be effectively driven by human mechanical actions (frequency lower than 20 Hz), showing great potential in wearable health monitoring systems. But this memory device may not be suitable for high-frequency applications that need a fast erasing process in parallel.

Soft robot integrated with multiple sensors is another hot research topic, which shows a bright future in artificial intelligence.[262–265] Living organisms could sense and respond to the varied environment through reflection-driven approaches.

**ADVANCED
SCIENCE NEWS**

www.advancedsciencenews.com

**ADVANCED
FUNCTIONAL
MATERIALS**

www.afm-journal.de

Figure 13. Active sensors for speech recognition and artificial synapses. a) Schematic illustration of the promising applications of voice user interface platform. Reproduced with permission.[237] Copyright 2019, Wiley-VCH GmbH. b) Schematic illustration of the overall concept of the basilar membrane inspired flexible piezoelectric acoustic sensor (f-PAS). Reproduced with permission.[246] Copyright 2018, Elsevier Ltd. c) Conceptual schematics of organ of Corti in mammalian cochlea. Thin PZT film was placed under BM, and vibrates in the same manner as BM according to sound wave. When a tensile stress was applied parallel to the surface of PZT film, the PZT film was bent upward with a height of 600 nm and generated piezopotential of ≈3 V. Reproduced with permission.[247] Copyright 2014, Wiley-VCH GmbH. d) The biological sensory nerve system. The mechanoreceptors in human skin receive mechanical stimulus and convert it into the presynaptic potentials. The presynaptic potentials are transmitted to the central nervous system through neurons and synapses. Reproduced with permission.[258] Copyright 2019, Wiley-VCH GmbH.

One great challenge for imutating such natural intelligence in robots is to develop sophisticated actuation/sensing mechanisms and achieve highly integrated multifunctionality.[266–270] Moreover, the soft robot promises as a candidate for emerging applications on various in vivo/vitro biomedical occasions.[271,272] As depicted in **Figure 14**a, Wang et al. presented a smart thin-film composite-based somatosensory light-driven robots (SLiRs), which combined the actuation and multiple sensors.[273] The SLiR integrated piezoresistive strain sensation and pyro/piezoelectric responses driven by a photo actuator transducer, enabling concurrently and noninterfering detection

of its actuation deformation states and body temperature. The SLiR could not only move forward on surfaces in different roughness, but also provide feedback on its subtle terrain textures and detailed locomotive gaits. When it was fabricated into an artificial hand, the SLiR anthropomorphic hand showed multifunctional sensing based on the pyro/piezoelectric effect that was arisen from integrated mechanoreception, thermoreception, proprioception, and photoreception. This SLiR possesses capacities of both perception and motility, offering new opportunities for developing multiple sensory systems with diverse intelligent behaviors.
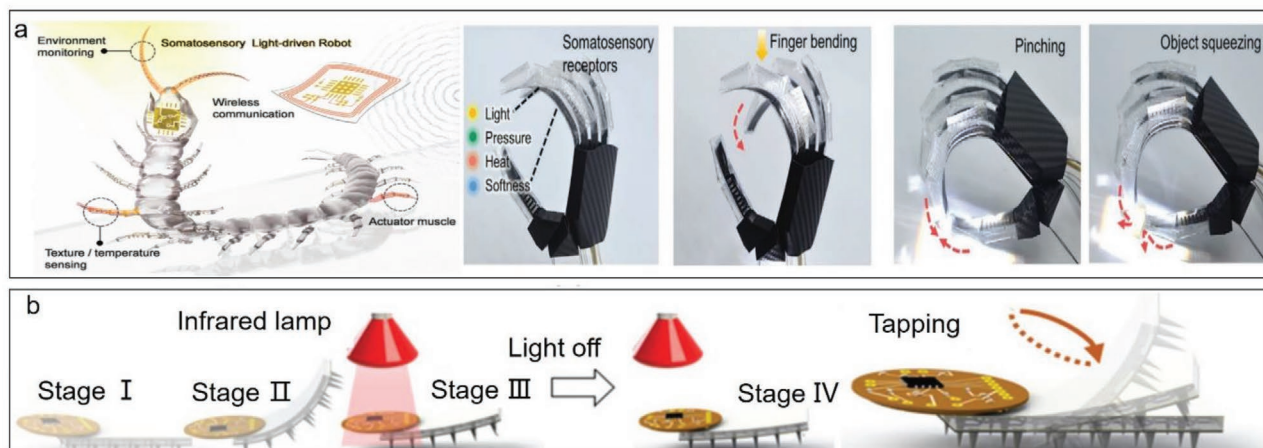
Figure 14. Active sensors based on piezoelectric effect for smart soft robot that can move, sense, and communicate remotely. a) The somatosensory light-driven robot (SLiR) anthropomorphic hand with intelligence inspired by a real hand. The five fingers are akin to somatosensory receptors: photoreceptor, mechanoreceptor, thermoreceptor, and proprioceptor, related to the specific stimuli triggered receptor. Reproduced with permission.[167] Copyright 2019, Elsevier Ltd. b-i) Wireless thermal sensing with different signal feedback under four stages in carried-on mode. Reproduced with permission.[272] Copyright 2017, Wiley-VCH. When the robot approaches the infrared lamp lighting area from a distance, the sensor signal rises from ≈24 to ≈40 °C. ii) Signal feedback of the in situ wireless tapping sensing on a flat rigid ground in carried-on mode. Reproduced with permission.[274] Copyright 2020, The Authors. Published by Wiley-VCH GmbH.

Figure 14b demonstrates another batteryless soft millirobot presented by Lu et al.[274] Based on the magnetic and piezoelectric effects, the millirobot can achieve moving, perceiving and communicating remotely. The proposed robot can perform carried-on sensing mode, where the surrounding information is instantaneity measured by the sensors located on the robot. To better demonstrate the feasibility, environment temperature was measured when the robot was walking based on the piezoelectric effect. Furthermore, the robot can achieve the wireless sensation of the tapping actions on the flat rigid ground. This research represented a significant progress in the emerging field of untethered soft robotics, which is conducive to a wide range of biomedical applications, such as diagnosis, in-body monitoring, and drug delivery.

5. Conclusion and Outlook

In this review, we introduce the rapid development of materials, fabrication, performance enhancement in the field of PENGs, and their applications in mechanical energy harvesting and self-powered multifunctional sensors. Ever since the invention of PENGs, its rapid development has inspired many research fields from energy harvesting to self-powered systems. On one hand, substantial efforts have been devoted to enhancing the output performance of PENGs, achieving several orders of magnitude enhancement. On the other hand, PENGs can be integrated with existing sensor equipment to build a self-powered system. Each device can work independently, and device arrays can form a network for real-time monitoring. Besides, it can serve as an active sensor that is self-powered for sensing most mechanical motions. Recent studies have demonstrated the great potential applications based on self-powered multifunctional sensors in microelectronic devices, devices in the biomedical field, human–computer interaction, intelligent robotics, and other fields. It is foreseeable that more

significance will be achieved by further development of this technology, which will have a dramatic impact not only on the field of wireless sensor networks, but also on our daily lives.

As a rapidly emerging micro–nanoenergy source, triboelectric nanogenerators (TENGs) have been intensively investigated and extended to many research fields from energy sources to sensors in recent years. However, the large internal resistance in TENG inevitably leads to a limited output current, thus reduces the total output power and energy conversion efficiency.[275,276] Therefore, it is an effective way to developing advanced multifunctional induction and self-powered flexible equipment by integrating both TENGs and PENGs, thereby helping to overcome the corresponding limitations. Moreover, with the rapid development of TENG in recent years, its research directions have mainly involved four areas: 1) micro/nanoenergy sources for small and mobile electronics; 2) active sensing for tactile touch,[174] acoustic sensing,[277] acceleration,[278] chemical sensing,[279] and even the development of advanced HMI;[280] 3) blue energy, which means harvesting the kinetic energy of water waves in the vast oceans; 4) direct high voltage power sources application such as exciting plasma, field emission, etc. Therefore, we can try to find new development opportunities and space, looking back to the development of PENGs and targeting new development directions such as high-power sources, self-powered sensor system, etc. Although considerable achievements in self-powered sensors have been demonstrated, practical applications are still faced with emerging and grand challenges. In the future research process, further development of self-powered multifunctional sensors needs to consider the following aspects.

1. The energy output performance and energy conversion efficiency of the flexible PENGs: For the self-powered sensor system, the energy density of energy suppliers is a key parameter, which plays an important role in the continuous and stable operation of the entire system. Therefore, scientists

need to continuously enhance the performance of PENG as a self-powered sensor. New materials and device structures are also encouraged to be designed so as to achieve more practical applicability in wireless sensor networks. For instance, developing materials with nano–microscopic morphologies, functionalization by doping with chemical elements and surface modification process call for more attempts to achieve a higher energy density, which will further improve the sensitivity of active sensors. Furthermore, we propose to synthesize composite materials by mixing inorganic piezoelectric materials and organic polymers, combining the high piezoelectric coefficient of inorganic materials and the good flexibility of organic polymers. This strategy will not only help to synthesize flexible piezoelectric materials, but also benefit from both piezoelectric effects of inorganic materials and organic polymers to achieve higher output performance.

2. System integration: For future practical applications, researchers can work on the perspective of integrated sensors to achieve multiple functions at the same time and realize artificial intelligence applications by combining machine learning and remote control. In addition, developing the integration with other modules in sensor systems and realizing self-powered operation for entire wireless sensor nodes including the supporting components will eventually promote the use of PENGs as active self-powered sensors in wireless sensor networks.

3. Durability of the materials and devices: According to the application scenarios of sensors, flexible active sensors have been developed, but they will deform repeatedly in actual use and affect the performance of the device, eventually seriously reducing the detection accuracy and service life of the equipment. Researchers can make greater efforts in packaging materials and packaging technology to improve the stability and durability of devices. For instance, choosing excellent elasticity and superior mechanical properties materials such as polydimethylsiloxane to package the sensor device for the enhancement of durability.

Overall, since studies on the self-powered sensor are still in the early stage, great attention should be paid to the improvement of size, sensitivity, flexibility, long-term stability, and integration. Although these challenges still exist, through the continuous research on self-powered active sensors based on PENGs in the next few years to further improve the sensitivity and achieve the self-powered operation of the entire sensor node system, they will soon be widely used in portable electronic devices, electronic skin, signal conversion, biomedical, artificial intelligence, and more.

Conflict of Interest

The authors declare no conflict of interest.

[1] Z. L. Wang, J. Song, *Science* **2006**, *312*, 242.
[2] Z. L. Wang, G. Zhu, Y. Yang, S. Wang, C. Pan, *Mater. Today* **2012**, *15*, 532.
[3] Z. L. Wang, *ACS Nano* **2013**, *7*, 9533.
[4] Y. F. Hu, Z. L. Wang, *Nano Energy* **2015**, *14*, 3.
[5] Z. Zhao, Y. Dai, S. X. Dou, J. Liang, *Mater. Today Energy* **2021**, *20*, 100690.
[6] D. Hu, M. Yao, Y. Fan, C. Ma, M. Fan, M. Liu, *Nano Energy* **2019**, *55*, 288.
[7] Y. Liu, R. Bao, J. Tao, J. Li, M. Dong, C. Pan, *Sci. Bull.* **2020**, *65*, 70.
[8] J. Curie, P. Curie, *Bull. Mineral.* **1880**, *3*, 90.
[9] S. R. Anton, H. A. Sodano, *Smart Mater. Struct.* **2007**, *16*, R1.
[10] H. S. Kim, J.-H. Kim, J. Kim, *Int. J. Precis. Eng. Manuf.* **2011**, *12*, 1129.
[11] A. Khan, M. A. Abbasi, J. Wissting, O. Nur, M. Willander, *Phys. Status Solidi RRL* **2013**, *7*, 980.
[12] W. L. Deng, T. Yang, L. Jin, C. Yan, H. C. Huang, X. Chu, Z. X. Wang, D. Xiong, G. Tian, Y. Y. Gao, H. T. Zhang, W. Q. Yang, *Nano Energy* **2019**, *55*, 516.
[13] F. R. Fan, W. Tang, Z. L. Wang, *Adv. Mater.* **2016**, *28*, 4283.
[14] L.-L. Xing, C.-H. Ma, Z.-H. Chen, Y.-J. Chen, X.-Y. Xue, *Nanotechnology* **2011**, *22*, 215501.
[15] Z. Gao, J. Zhou, Y. Gu, P. Fei, Y. Hao, G. Bao, Z. L. Wang, *J. Appl. Phys.* **2009**, *105*, 113707.
[16] W. Deng, T. Yang, L. Jin, C. Yan, H. Huang, X. Chu, Z. Wang, D. Xiong, G. Tian, Y. Gao, H. Zhang, W. Yang, *Nano Energy* **2019**, *55*, 516.
[17] B. Liu, M. Wang, M. Chen, J. Wang, J. Liu, D. Hu, S. Liu, X. Yao, H. Yang, *ACS Appl. Mater. Interfaces* **2019**, *11*, 12656.
[18] R. Pandey, N. P. Maria Joseph Raj, V. Singh, P. Iyamperumal Anand, S. J. Kim, *ACS Appl. Mater. Interfaces* **2019**, *11*, 6078.
[19] D.-M. S. Gyu Han Kim, H.-K. Kim, Y.-H. Hwang, *J. Korean Phys. Soc.* **2015**, *67*, 1920.
[20] J. Zhao, Z.-G. Jin, X.-X. Liu, Z.-F. Liu, *J. Eur. Ceram. Soc.* **2006**, *26*, 3745.
[21] G. Hua, Y. Zhang, J. Zhang, X. Cao, W. Xu, L. Zhang, *Mater. Lett.* **2008**, *62*, 4109.
[22] H. Zhu, Y. Wang, J. Xiao, M. Liu, S. Xiong, Z. J. Wong, Z. Ye, Y. Ye, X. Yin, X. Zhang, *Nat. Nanotechnol.* **2015**, *10*, 151.
[23] T. Cao, G. Wang, W. Han, H. Ye, C. Zhu, J. Shi, Q. Niu, P. Tan, E. Wang, B. Liu, J. Feng, *Nat. Commun.* **2012**, *3*, 887.
[24] S. K. Ghosh, D. Mandal, *Piezoelectricity of 2D Materials and its Applications toward Mechanical Energy Harvesting.* In 2D Nanomaterials for Energy Applications **2020**, pp. 1–38.
[25] W. Wu, L. Wang, Y. Li, F. Zhang, L. Lin, S. Niu, D. Chenet, X. Zhang, Y. Hao, T. F. Heinz, J. Hone, Z. L. Wang, *Nature* **2014**, *514*, 470.
[26] H. Song, I. Karakurt, M. Wei, N. Liu, Y. Chu, J. Zhong, L. Lin, *Nano Energy* **2018**, *49*, 7.
[27] G. Da Cunha Rodrigues, P. Zelenovskiy, K. Romanyuk, S. Luchkin, Y. Kopelevich, A. Kholkin, *Nat. Commun.* **2015**, *6*, 7572.

ADVANCED
SCIENCE NEWS
www.advancedsciencenews.com

ADVANCED
FUNCTIONAL
MATERIALS
www.afm-journal.de

[28] K.-A. N. Duerloo, M. T. Ong, E. J. Reed, *J. Phys. Chem. Lett.* **2012**, *3*, 2871.

[29] K. H. Michel, B. Verberck, *Phys. Rev. B* **2009**, *80*, 224301.

[30] M. T. Ong, E. J. Reed, *ACS Nano* **2012**, *6*, 1387.

[31] F. Xue, J. Zhang, W. Hu, W. T. Hsu, A. Han, S. F. Leung, J. K. Huang, Y. Wan, S. Liu, J. Zhang, J. H. He, W. H. Chang, Z. L. Wang, X. Zhang, L. J. Li, *ACS Nano* **2018**, *12*, 4976.

[32] A. Y. Lu, H. Zhu, J. Xiao, C. P. Chuu, Y. Han, M. H. Chiu, C. C. Cheng, C. W. Yang, K. H. Wei, Y. Yang, Y. Wang, D. Sokaras, D. Nordlund, P. Yang, D. A. Muller, M. Y. Chou, X. Zhang, L. J. Li, *Nat. Nanotechnol.* **2017**, *12*, 744.

[33] J. H. Lee, J. Y. Park, E. B. Cho, T. Y. Kim, S. A. Han, T. H. Kim, Y. Liu, S. K. Kim, C. J. Roh, H. J. Yoon, H. Ryu, W. Seung, J. S. Lee, J. Lee, S. W. Kim, *Adv. Mater.* **2017**, *29*, 1606667.

[34] W. Jin, Z. Wang, H. Huang, X. Hu, Y. He, M. Li, L. Li, Y. Gao, Y. Hu, H. Gu, *RSC Adv.* **2018**, *8*, 7422.

[35] S. Zhang, X. Lin, H. Liu, Z. Yuan, Y. Huan, X. Yuan, S. Huang, X. Cheng, *Int. J. Energy Res.* **2020**, *45*, 6213.

[36] S. H. Shin, S. Y. Choi, M. H. Lee, J. Nah, *ACS Appl. Mater. Interfaces* **2017**, *9*, 41099.

[37] G. Jian, Y. Jiao, Q. Meng, H. Shao, F. Wang, Z. Wei, *Adv. Mater. Interfaces* **2020**, *7*, 2070089.

[38] J. B. Yu, X. J. Hou, M. Cui, N. Zhang, S. N. Zhang, J. He, X. J. Chou, *Mater. Lett.* **2020**, *269*, 127686.

[39] P. A. Wlodkowski, K. Deng, M. Kahn, *Sens. Actuators, A* **2001**, *90*, 125.

[40] V. S. Nguyen, D. Rouxel, B. Vincent, L. Badie, F. D. D. Santos, E. Lamouroux, Y. Fort, *Appl. Surf. Sci.* **2013**, *279*, 204.

[41] Y. Qi, M. C. McAlpine, *Energy Environ. Sci.* **2010**, *3*, 1275.

[42] G. Zhu, A. C. Wang, Y. Liu, Y. Zhou, Z. L. Wang, *Nano Lett.* **2012**, *12*, 3086.

[43] L. Persano, C. Dagdeviren, Y. Su, Y. Zhang, S. Girardo, D. Pisignano, Y. Huang, J. A. Rogers, *Nat. Commun.* **2013**, *4*, 1633.

[44] G.-T. Hwang, V. Annapureddy, J. H. Han, D. J. Joe, C. Baek, D. Y. Park, D. H. Kim, J. H. Park, C. K. Jeong, K.-I. Park, J.-J. Choi, D. K. Kim, J. Ryu, K. J. Lee, *Adv. Energy Mater.* **2016**, *6*, 1600237.

[45] H. Kawai, *Jpn. J. Appl. Phys.* **1969**, *8*, 975.

[46] S. Egusa, Z. Wang, N. Chocat, Z. M. Ruff, A. M. Stolyarov, D. Shemuly, F. Sorin, P. T. Rakich, J. D. Joannopoulos, Y. Fink, *Nat. Mater.* **2010**, *9*, 643.

[47] H. Sun, H. Tian, Y. Yang, D. Xie, Y. C. Zhang, X. Liu, S. Ma, H. M. Zhao, T. L. Ren, *Nanoscale* **2013**, *5*, 6117.

[48] J. Fang, X. Wang, T. Lin, *J. Mater. Chem.* **2011**, *21*, 11088.

[49] Z. H. Liu, C. T. Pan, L. W. Lin, J. C. Huang, Z. Y. Ou, *Smart Mater. Struct.* **2014**, *23*, 025003.

[50] A. J. Lovinger, *Science* **1983**, *220*, 1115.

[51] G. Zhu, Z. Zeng, L. Zhang, X. Yan, *Comput. Mater. Sci.* **2008**, *44*, 224.

[52] S. K. Karan, R. Bera, S. Paria, A. K. Das, S. Maiti, A. Maitra, B. B. Khatua, *Adv. Energy Mater.* **2016**, *6*, 1601016.

[53] A. Pal, A. Sasmal, B. Manoj, D. S. D. P. Rao, A. K. Haldar, S. Sen, *Mater. Chem. Phys.* **2020**, *244*, 122639.

[54] N. Chakhchaoui, R. Farhan, A. Eddiai, M. Meddad, O. Cherkaoui, M. Mazroui, Y. Boughaleb, L. Van Langenhove, *Mater. Today: Proc.* **2020**, *39*, 1148.

[55] S. H. Wankhade, S. Tiwari, A. Gaur, P. Maiti, *Energy Rep.* **2020**, *6*, 358.

[56] Z. Pi, J. Zhang, C. Wen, Z.-b. Zhang, D. Wu, *Nano Energy* **2014**, *7*, 33.

[57] E. J. Ko, S. J. Jeon, Y. W. Han, S. Y. Jeong, C. Y. Kang, T. H. Sung, K. W. Seong, D. K. Moon, *Nano Energy* **2019**, *58*, 11.

[58] J. Liu, B. Yang, L. J. Lu, X. L. Wang, X. Y. Li, X. Chen, J. Q. Liu, *Sens. Actuat.* **2020**, *303*, 111796.

[59] Q. Zhao, L. Yang, K. Chen, Y. Ma, Q. Peng, H. Ji, J. Qiu, *Compos. Sci. Technol.* **2020**, *199*, 108330.

[60] J. Ryu, J. Kim, J. Oh, S. Lim, J. Y. Sim, J. S. Jeon, K. No, S. Park, S. Hong, *Nano Energy* **2019**, *55*, 348.

[61] Y. Han, C. Jiang, H. Lin, C. Luo, R. Qi, H. Peng, *Energy Technol.* **2020**, *8*, 1901249.

[62] T. Yang, H. Pan, G. Tian, B. Zhang, D. Xiong, Y. Gao, C. Yan, X. Chu, N. Chen, S. Zhong, L. Zhang, W. Deng, W. Yang, *Nano Energy* **2020**, *72*, 104706.

[63] T. Yucel, P. Cebe, D. L. Kaplan, *Adv. Funct. Mater.* **2011**, *21*, 779.

[64] C. W. Marvin, H. M. Grimm, N. C. Miller, W. S. Horne, G. R. Hutchison, *J. Phys. Chem. B* **2017**, *121*, 10269.

[65] B. Y. Lee, J. Zhang, C. Zueger, W. J. Chung, S. Y. Yoo, E. Wang, J. Meyer, R. Ramesh, S. W. Lee, *Nat. Nanotechnol.* **2012**, *7*, 351.

[66] J. H. Lee, K. Heo, K. Schulz-Schonhagen, J. H. Lee, M. S. Desai, H. E. Jin, S. W. Lee, *ACS Nano* **2018**, *12*, 8138.

[67] C. Kumar, A. Gaur, S. Tiwari, A. Biswas, S. K. Rai, P. Maiti, *Compos. Commun.* **2019**, *11*, 56.

[68] S. Rajala, T. Siponkoski, E. Sarlin, M. Mettänen, M. Vuoriluoto, A. Pammo, J. Juuti, O. J. Rojas, S. Franssila, S. Tuukkanen, *ACS Appl. Mater. Interfaces* **2016**, *8*, 15607.

[69] G. Zhang, Q. Liao, Z. Zhang, Q. Liang, Y. Zhao, X. Zheng, Y. Zhang, *Adv. Sci.* **2016**, *3*, 1500257.

[70] R. D. B. Fraser, T. P. Macrae, E. Suzuki, *J. Mol. Biol.* **1979**, *129*, 463.

[71] S. Sun, T. Kou, H. Zhu, *J. Appl. Polym. Sci.* **1997**, *64*, 267.

[72] T. Ikoma, H. Kobayashi, J. Tanaka, D. Walsh, S. Mann, *Int. J. Biol. Macromol.* **2003**, *32*, 199.

[73] S. K. Ghosh, D. Mandal, *Appl. Phys. Lett.* **2016**, *109*, 232.

[74] S. K. Ghosh, D. Mandal, *Nano Energy* **2016**, *28*, 356.

[75] C. Ribeiro, V. Sencadas, D. M. Correia, S. Lanceros-Mendez, *Colloids Surf., B* **2015**, *136*, 46.

[76] S. K. Mahadeva, K. Walus, B. Stoeber, *ACS Appl. Mater. Interfaces* **2014**, *6*, 7547.

[77] G. Helenius, H. Backdahl, A. Bodin, U. Nannmark, P. Gatenholm, B. Risberg, *J. Biomed. Mater. Res., Part A* **2006**, *76*, 431.

[78] J. Shah, R. M. BrownJr., *Appl. Microbiol. Biotechnol.* **2005**, *66*, 352.

[79] S. Maiti, S. K. Karan, J. Lee, A. K. Mishra, B. B. Khatua, J. K. Kim, *Nano Energy* **2017**, *42*, 282.

[80] E. N. Harvey, *Science* **1939**, *89*, 460.

[81] G. H. Altman, F. Diaz, C. Jakuba, T. Calabro, R. L. Horan, J. Chen, H. Lu, J. Richmond, D. L. Kaplan, *Biomaterials* **2003**, *24*, 401.

[82] S. K. Karan, S. Maiti, O. Kwon, S. Paria, A. Maitra, S. K. Si, Y. Kim, J. K. Kim, B. B. Khatua, *Nano Energy* **2018**, *49*, 655.

[83] S. Lee, S.-H. Bae, L. Lin, Y. Yang, C. Park, S.-W. Kim, S. N. Cha, H. Kim, Y. J. Park, Z. L. Wang, *Adv. Funct. Mater.* **2013**, *23*, 2445.

[84] G. M. Hasan Ul Banna, I. K. Park, *Nanotechnology* **2017**, *28*, 445402.

[85] L. Lin, C. H. Lai, Y. Hu, Y. Zhang, X. Wang, C. Xu, R. L. Snyder, L. J. Chen, Z. L. Wang, *Nanotechnology* **2011**, *22*, 475401.

[86] J. K. Han, S. Kim, S. Jang, Y. R. Lim, S. W. Kim, H. Chang, W. Song, S. S. Lee, J. Lim, K. S. An, S. Myung, *Nano Energy* **2019**, *61*, 471.

[87] X. Niu, W. Jia, S. Qian, J. Zhu, J. Zhang, X. Hou, J. Mu, W. Geng, J. Cho, J. He, X. Chou, *ACS Sustainable Chem. Eng.* **2018**, *7*, 979.

[88] S. K. Karan, D. Mandal, B. B. Khatua, *Nanoscale* **2015**, *7*, 10655.

[89] H. Zhang, S. Jiang, J. Xiao, K. Kajiyoshi, *J. Appl. Phys.* **2010**, *107*, 124118.

[90] Y. Sun, W. Luo, *J. Food, Agric. Environ.* **2013**, *11*, 1097.

[91] K. Saigusa, T. Morita, *Jpn. J. Appl. Phys.* **2016**, *55*, 07KC05.

[92] H. Wu, Z. Hu, B. Li, H. Wang, Y. Peng, D. Zhou, X. Zhang, *Mater. Lett.* **2015**, *161*, 565.

[93] H. J. Jung, S. Lee, Y. Yu, S. M. Hong, H. C. Choi, M. Y. Choi, *Thin Solid Films* **2012**, *524*, 144.

[94] S. Pati, *J. Alloys Compd.* **2017**, *695*, 3552.

[95] S. H. Kim, S. Komarneni, *Ceram. Int.* **2011**, *37*, 1101.

**ADVANCED
SCIENCE NEWS**

www.advancedsciencenews.com

**ADVANCED
FUNCTIONAL
MATERIALS**

www.afm-journal.de

[96] D. Wang, J. Ou-Yang, W. Guo, X. Yang, B. Zhu, *Ceram. Int.* **2017**, *43*, 9573.

[97] X. Wang, F. Wang, L. Qi, R. Guo, B. Li, D. Chen, H. Zou, *Ceram. Int.* **2020**, *46*, 10256.

[98] M. Wang, W. Ma, N. Chen, Y. Guo, J. Ma, Z. Zhao, *Mater. Lett.* **2015**, *152*, 17.

[99] Y. Sun, Q. Wang, L. Qin, in 2013 IEEE Int. Ultrasonics Symp. (IUS), IEEE, Piscataway, NJ **2013**, pp. 1097–1100.

[100] F. Gheorghiu, R. Apetrei, M. Dobromir, A. Ianculescu, D. Luca, L. Mitoseriu, *Process. Appl. Ceram.* **2014**, *8*, 113.

[101] H. Wu, Z. Hu, B. Li, H. Wang, D. Zhou, X. Zhang, *Mater. Lett.* **2018**, *232*, 206.

[102] J. Ding, S. Chen, N. Han, Y. Shi, P. Hu, H. Li, J. Wang, *Ceram. Int.* **2020**, *46*, 15152.

[103] C.-Q. Luo, F. C.-C. Ling, M. A. Rahman, M. Phillips, C. Ton-That, C. Liao, K. Shih, J. Lin, H. W. Tam, A. B. Djurišić, S.-P. Wang, *Appl. Surf. Sci.* **2019**, *483*, 1129.

[104] D. Kumar, R. S. Rai, N. K. Singh, *Ceram. Int.* **2020**, *46*, 26216.

[105] M. Shaheera, K. G. Girija, M. Kaur, V. Geetha, A. K. Debnath, R. K. Vatsa, K. P. Muthe, S. C. Gadkari, *Opt. Mater.* **2020**, *101*, 109723.

[106] A. N. Filippin, J. R. Sanchez-Valencia, X. Garcia-Casas, V. Lopez-Flores, M. Macias-Montero, F. Frutos, A. Barranco, A. Borras, *Nano Energy* **2019**, *58*, 476.

[107] J. H. Jung, M. Lee, J. I. Hong, Y. Ding, C. Y. Chen, L. J. Chou, Z. L. Wang, *ACS Nano* **2011**, *5*, 10041.

[108] M. Koç, L. Paralı, O. Şan, *Polym. Test.* **2020**, *90*, 106695.

[109] X. Guan, B. Xu, J. Gong, *Nano Energy* **2020**, *70*, 104516.

[110] X. Wei, Y. Liu, D. Zhao, S. S. Ge, *J. Eur. Ceram. Soc.* **2020**, *40*, 5423.

[111] D. Yao, H. Cui, R. Hensleigh, P. Smith, S. Alford, D. Bernero, S. Bush, K. Mann, H. F. Wu, M. Chin-Nieh, G. Youmans, X. Zheng, *Adv. Funct. Mater.* **2019**, *29*, 1903866.

[112] X. Zhou, K. Parida, O. Halevi, Y. Liu, J. Xiong, S. Magdassi, P. S. Lee, *Nano Energy* **2020**, *72*, 104676.

[113] Y. Y. Zhuang, S. Han, W. H. Liu, X. Y. Wei, Z. Xu, *J. Alloys Compd.* **2020**, *831*, 154657.

[114] L. Zhang, J. Gui, Z. Wu, R. Li, Y. Wang, Z. Gong, X. Zhao, C. Sun, S. Guo, *Nano Energy* **2019**, *65*, 103924.

[115] J. Ma, Z. Shi, C. W. Nan, *Adv. Mater.* **2007**, *19*, 2571.

[116] K.-I. Park, C. K. Jeong, J. Ryu, G.-T. Hwang, K. J. Lee, *Adv. Energy Mater.* **2013**, *3*, 1539.

[117] I. Fujii, K. Nakashima, N. Kumada, S. Wada, *J. Ceram. Soc. Jpn.* **2012**, *120*, 30.

[118] Z.-H. Lin, Y. Yang, J. M. Wu, Y. Liu, F. Zhang, Z. L. Wang, *J. Phys. Chem. Lett.* **2012**, *3*, 3599.

[119] C. Liu, A. Yu, M. Peng, M. Song, W. Liu, Y. Zhang, J. Zhai, *J. Phys. Chem. C* **2016**, *120*, 6971.

[120] V. Bhavanasi, V. Kumar, K. Parida, J. Wang, P. S. Lee, *ACS Appl. Mater. Interfaces* **2016**, *8*, 521.

[121] S. Lee, J. Lee, W. Ko, S. Cha, J. Sohn, J. Kim, J. Park, Y. Park, J. Hong, *Nanoscale* **2013**, *5*, 9609.

[122] D. Zhu, T. Hu, Y. Zhao, W. Zang, L. Xing, X. Xue, *Sens. Actuators, B* **2015**, *213*, 382.

[123] T. Zhao, Y. Fu, Y. Zhao, L. Xing, X. Xue, *J. Alloys Compd.* **2015**, *648*, 571.

[124] K. I. Park, M. Lee, Y. Liu, S. Moon, G. T. Hwang, G. Zhu, J. E. Kim, S. O. Kim, D. K. Kim, Z. L. Wang, K. J. Lee, *Adv. Mater.* **2012**, *24*, 2999.

[125] Y. Zhang, M. Wu, Q. Zhu, F. Wang, H. Su, H. Li, C. Diao, H. Zheng, Y. Wu, Z. L. Wang, *Adv. Funct. Mater.* **2019**, *29*, 1904259.

[126] H. Patnam, B. Dudem, N. R. Alluri, A. R. Mule, S. A. Graham, S. J. Kim, J. S. Yu, *Compos. Sci. Technol.* **2020**, *188*, 107963.

[127] R. Sahoo, S. Mishra, L. Unnikrishnan, S. Mohanty, S. Mahapatra, S. K. Nayak, S. Anwar, A. Ramadoss, *Mater. Sci. Semicond. Process.* **2020**, *117*, 105173.

[128] A. R. Chowdhury, A. M. Abdullah, I. Hussain, J. Lopez, D. Cantu, S. K. Gupta, Y. Mao, S. Danti, M. J. Uddin, *Nano Energy* **2019**, *61*, 327.

[129] N. Sinha, G. Ray, S. Bhandari, S. Godara, B. Kumar, *Ceram. Int.* **2014**, *40*, 12337.

[130] L. Kang, H. An, J. Y. Park, M. H. Hong, S. Nahm, C. G. Lee, *Appl. Surf. Sci.* **2019**, *475*, 969.

[131] S. Goel, B. Kumar, *J. Alloys Compd.* **2020**, *816*, 152491.

[132] M. M. Alam, D. Mandal, *ACS Appl. Mater. Interfaces* **2016**, *8*, 1555.

[133] C.-L. Hsu, I. L. Su, T.-J. Hsueh, *RSC Adv.* **2015**, *5*, 34019.

[134] Y. Zhang, C. Liu, J. Liu, J. Xiong, J. Liu, K. Zhang, Y. Liu, M. Peng, A. Yu, A. Zhang, Y. Zhang, Z. Wang, J. Zhai, Z. L. Wang, *ACS Appl. Mater. Interfaces* **2016**, *8*, 1381.

[135] K. Batra, N. Sinha, B. Kumar, *Ceram. Int.* **2020**, *46*, 24120.

[136] Y. H. Kwon, D.-H. Kim, H.-K. Kim, J. Nah, *Nano Energy* **2015**, *18*, 126.

[137] G. Zhang, Q. Liao, M. Ma, F. Gao, Z. Zhang, Z. Kang, Y. Zhang, *Nano Energy* **2018**, *52*, 501.

[138] C. R. Jin, N. J. Hao, Z. Xu, I. Trase, Y. Nie, L. Dong, A. Closson, Z. Chen, J. X. J. Zhang, *Sens. Actuators, A* **2020**, *305*, 111912.

[139] Q. Y. Wang, D. C. Yang, Y. Qiu, X. T. Zhang, W. B. Song, L. Z. Hu, *Appl. Phys. Lett.* **2018**, *112*, 5.

[140] L. Yang, H. Ji, K. Zhu, J. Wang, J. Qiu, *Compos. Sci. Technol.* **2016**, *123*, 259.

[141] A. Anand, M. C. Bhatnagar, *Mater. Today Energy* **2019**, *13*, 293.

[142] S. Ye, C. Cheng, X. Chen, X. Chen, J. Shao, J. Zhang, H. Hu, H. Tian, X. Li, L. Ma, W. Jia, *Nano Energy* **2019**, *60*, 701.

[143] H. Shao, J. Fang, H. Wang, C. Lang, T. Lin, *ACS Appl. Mater. Interfaces* **2015**, *7*, 22551.

[144] L. B. Huang, W. Xu, J. Hao, *Small* **2017**, *13*, 1701820.

[145] S. Ma, T. Ye, T. Zhang, Z. Wang, K. Li, M. Chen, J. Zhang, Z. Wang, S. Ramakrishna, L. Wei, *Adv. Mater. Technol.* **2018**, *3*, 1800033.

[146] J. Fang, H. Niu, H. Wang, X. Wang, T. Lin, *Energy Environ. Sci.* **2013**, *6*, 2196.

[147] C. Zhao, J. Niu, Y. Zhang, C. Li, P. Hu, *Composites, Part B* **2019**, *178*, 107447.

[148] C. Chen, Z. Bai, Y. Cao, M. Dong, K. Jiang, Y. Zhou, Y. Tao, S. Gu, J. Xu, X. Yin, W. Xu, *Compos. Sci. Technol.* **2020**, *192*, 108100.

[149] S. K. Ghosh, D. Mandal, *Nano Energy* **2018**, *53*, 245.

[150] B. Kumar, K. Y. Lee, H. K. Park, S. J. Chae, Y. H. Lee, S. W. Kim, *ACS Nano* **2011**, *5*, 4197.

[151] Q. Wang, D. Yang, Y. Qiu, X. Zhang, W. Song, L. Hu, *Appl. Phys. Lett.* **2018**, *112*, 063906.

[152] A. Khan, M. A. Abbasi, M. Hussain, Z. Hussain Ibupoto, J. Wissting, O. Nur, M. Willander, *Appl. Phys. Lett.* **2012**, *101*, 193506.

[153] G. Zhu, R. Yang, S. Wang, Z. L. Wang, *Nano Lett.* **2010**, *10*, 3151.

[154] Z. H. Lin, Y. Yang, J. M. Wu, Y. Liu, F. Zhang, Z. L. Wang, *J. Phys. Chem. Lett.* **2012**, *3*, 3599.

[155] K. I. Park, S. B. Bae, S. H. Yang, H. I. Lee, K. Lee, S. J. Lee, *Nanoscale* **2014**, *6*, 8962.

[156] Q. L. Zhao, G. P. He, J. J. Di, W. L. Song, Z. L. Hou, P. P. Tan, D. W. Wang, M. S. Cao, *ACS Appl. Mater. Interfaces* **2017**, *9*, 24696.

[157] X. Chen, S. Xu, N. Yao, Y. Shi, *Nano Lett.* **2010**, *10*, 2133.

[158] M. Hussain, M. A. Abbasi, Z. H. Ibupoto, O. Nur, M. Willander, *Phys. Status Solidi A* **2014**, *211*, 455.

[159] Y. Hu, L. Lin, Y. Zhang, Z. L. Wang, *Adv. Mater.* **2012**, *24*, 110.

[160] N. Jalali, P. Woolliams, M. Stewart, P. M. Weaver, M. G. Cain, S. Dunn, J. Briscoe, *J. Mater. Chem. A* **2014**, *2*, 10945.

[161] S. A. Han, T. H. Kim, S. K. Kim, K. H. Lee, H. J. Park, J. H. Lee, S. W. Kim, *Adv. Mater.* **2018**, *30*, 1800342.

[162] Z. L. Wang, X. Y. Kong, Y. Ding, P. Gao, W. L. Hughes, R. Yang, Y. Zhang, *Adv. Funct. Mater.* **2004**, *14*, 943.

[163] Z. Qu, Y. Fu, B. Yu, P. Deng, L. Xing, X. Xue, *Sens. Actuators, B* **2016**, *222*, 78.

[164] B. Yin, Y. Qiu, H. Zhang, J. Lei, Y. Chang, J. Ji, Y. Luo, Y. Zhao, L. Hu, *Nano Energy* **2015**, *14*, 95.

[165] Y. Huan, X. S. Zhang, J. A. Song, Y. Zhao, T. Wei, G. G. Zhang, X. H. Wang, *Nano Energy* **2018**, *50*, 62.

[166] S. Siddiqui, D. I. Kim, E. Roh, L. T. Duy, T. Q. Trung, M. T. Nguyen, N. E. Lee, *Nano Energy* **2016**, *30*, 434.

[167] E. Kar, N. Bose, B. Dutta, S. Banerjee, N. Mukherjee, S. Mukherjee, *Energy Convers. Manage.* **2019**, *184*, 600.

[168] D. Ponnamma, H. Parangusan, A. Tanvir, M. A. AlMa'adeed, *Mater. Des.* **2019**, *184*, 108176.

[169] C. Dagdeviren, B. D. Yang, Y. Su, P. L. Tran, P. Joe, E. Anderson, J. Xia, V. Doraiswamy, B. Dehdashti, X. Feng, B. Lu, R. Poston, Z. Khalpey, R. Ghaffari, Y. Huang, M. J. Slepian, J. A. Rogers, *Proc. Natl. Acad. Sci. USA* **2014**, *111*, 1927.

[170] N. Li, Z. Yi, Y. Ma, F. Xie, Y. Huang, Y. Tian, X. Dong, Y. Liu, X. Shao, Y. Li, L. Jin, J. Liu, Z. Xu, B. Yang, H. Zhang, *ACS Nano* **2019**, *13*, 2822.

[171] Z. Liu, L. Xu, Q. Zheng, Y. Kang, B. Shi, D. Jiang, H. Li, X. Qu, Y. Fan, Z. L. Wang, Z. Li, *ACS Nano* **2020**, *14*, 8074.

[172] C. H. Yang, Y. Song, M. S. Woo, J. H. Eom, G. J. Song, J. H. Kim, J. Kim, T. H. Lee, J. Y. Choi, T. H. Sung, *Sens. Actuators, A* **2017**, *261*, 317.

[173] Y. Zhang, R. Zheng, K. Shimono, T. Kaizuka, K. Nakano, *Sensors* **2016**, *16*, 1727.

[174] S. Garain, S. Jana, T. K. Sinha, D. Mandal, *ACS Appl. Mater. Interfaces* **2016**, *8*, 4532.

[175] L. D. Du, Z. Fang, J. Z. Yan, Z. Zhao, *Sens. Actuators, A* **2017**, *260*, 35.

[176] J. Liu, H. Zuo, W. Xia, Y. Luo, D. Yao, Y. Chen, K. Wang, Q. Li, *Microelectron. Eng.* **2020**, *231*, 111333.

[177] C. L. Zhao, Q. Zhang, W. L. Zhang, X. Y. Du, Y. Zhang, S. B. Gong, K. L. Ren, Q. J. Sun, Z. L. Wang, *Nano Energy* **2019**, *57*, 440.

[178] C. Hu, L. Cheng, Z. Wang, Y. Zheng, S. Bai, Y. Qin, *Small* **2016**, *12*, 1315.

[179] C. Dagdeviren, P. Joe, O. L. Tuzman, K.-I. Park, K. J. Lee, Y. Shi, Y. Huang, J. A. Rogers, *Extreme Mech. Lett.* **2016**, *9*, 269.

[180] J. Li, X. Wang, *APL Mater.* **2017**, *5*, 073801.

[181] A. Wang, Z. Liu, M. Hu, C. Wang, X. Zhang, B. Shi, Y. Fan, Y. Cui, Z. Li, K. Ren, *Nano Energy* **2018**, *43*, 63.

[182] D. Jiang, B. Shi, H. Ouyang, Y. Fan, Z. L. Wang, Z. Li, *ACS Nano* **2020**, *14*, 6436.

[183] D. H. Kim, H. J. Shin, H. Lee, C. K. Jeong, H. Park, G.-T. Hwang, H.-Y. Lee, D. J. Joe, J. H. Han, S. H. Lee, J. Kim, B. Joung, K. J. Lee, *Adv. Funct. Mater.* **2017**, *27*, 1700341.

[184] S. H. Kondapalli, Y. Alazzawi, M. Malinowski, T. Timek, S. Chakrabartty, *IEEE Trans. Biomed. Circuits Syst.* **2018**, *12*, 1392.

[185] M. Han, H. Wang, Y. Yang, C. Liang, W. Bai, Z. Yan, H. Li, Y. Xue, X. Wang, B. Akar, H. Zhao, H. Luan, J. Lim, I. Kandela, G. A. Ameer, Y. Zhang, Y. Huang, J. A. Rogers, *Nat. Electron.* **2019**, *2*, 26.

[186] Y. Zhang, R. Zheng, K. Nakano, M. P. Cartmell, *Appl. Phys. Lett.* **2018**, *112*, 143901.

[187] Y. Hu, C. Xu, Y. Zhang, L. Lin, R. L. Snyder, Z. L. Wang, *Adv. Mater.* **2011**, *23*, 4068.

[188] J. Zhao, J. Yang, Z. Lin, N. Zhao, J. Liu, Y. Wen, P. Li, *Sens. Actuators, A* **2015**, *236*, 173.

[189] S. Orrego, K. Shoele, A. Ruas, K. Doran, B. Caggiano, R. Mittal, S. H. Kang, *Appl. Energy* **2017**, *194*, 212.

[190] Z. Wen, H. Guo, Y. Zi, M. H. Yeh, X. Wang, J. Deng, J. Wang, S. Li, C. Hu, L. Zhu, Z. L. Wang, *ACS Nano* **2016**, *10*, 6526.

[191] Y. Liu, N. Sun, J. Liu, Z. Wen, X. Sun, S. T. Lee, B. Sun, *ACS Nano* **2018**, *12*, 2893.

[192] J. M. Guo, R. M. Wen, J. Y. Zhai, Z. L. Wang, *Sci. Bull.* **2019**, *64*, 128.

[193] R. M. Fu, L. J. Tu, Y. H. Zhou, L. Fan, F. M. Zhang, Z. G. Wang, J. Xing, D. F. Chen, C. L. Deng, G. X. Tan, P. Yu, L. Zhou, C. Y. Ning, *Chem. Mater.* **2019**, *31*, 9850.

[194] X. Zhang, X. Shan, T. Xie, J. Miao, *Mech. Syst. Signal Process.* **2020**, *141*, 106476.

[195] S. Ahn, Y. Cho, S. Park, J. Kim, J. Sun, D. Ahn, M. Lee, D. Kim, T. Kim, H. Shin, J. J. Park, *Nano Energy* **2020**, *74*, 104932.

[196] K. Zhao, B. Ouyang, C. R. Bowen, Z. L. Wang, Y. Yang, *Nano Energy* **2020**, *71*, 104632.

[197] S. Lee, R. Hinchet, Y. Lee, Y. Yang, Z. H. Lin, G. Ardila, L. Montes, M. Mouis, Z. L. Wang, *Adv. Funct. Mater.* **2014**, *24*, 1163.

[198] J. Chun, N. R. Kang, J. Y. Kim, M. S. Noh, C. Y. Kang, D. Choi, S. W. Kim, Z. L. Wang, J. M. Baik, *Nano Energy* **2015**, *11*, 1.

[199] H. He, Y. Fu, W. Zang, Q. Wang, L. Xing, Y. Zhang, X. Xue, *Nano Energy* **2017**, *31*, 37.

[200] I. Kim, H. Roh, J. Yu, N. Jayababu, D. Kim, *ACS Energy Lett.* **2020**, *5*, 1577.

[201] Y. Yang, H. Pan, G. Xie, Y. Jiang, C. Chen, Y. Su, Y. Wang, H. Tai, *Sens. Actuators, A* **2020**, *301*, 111789.

[202] Z. Huo, X. Wang, Y. Zhang, B. Wan, W. Wu, J. Xi, Z. Yang, G. Hu, X. Li, C. Pan, *Nano Energy* **2020**, *73*, 104744.

[203] Q. Sun, W. Seung, B. J. Kim, S. Seo, S. W. Kim, J. H. Cho, *Adv. Mater.* **2015**, *27*, 3411.

[204] R. Zhang, M. Hummelgård, J. Örtegren, Y. Yang, H. Andersson, E. Balliu, N. Blomquist, M. Engholm, M. Olsen, Z. L. Wang, H. Olin, *Nano Energy* **2019**, *63*, 103842.

[205] T. He, H. Wang, J. Wang, X. Tian, F. Wen, Q. Shi, J. S. Ho, C. Lee, *Adv. Sci.* **2019**, *6*, 1901437.

[206] M. Zhu, Q. Shi, T. He, Z. Yi, Y. Ma, B. Yang, T. Chen, C. Lee, *ACS Nano* **2019**, *13*, 1940.

[207] D. H. Ho, Q. Sun, S. Y. Kim, J. T. Han, D. H. Kim, J. H. Cho, *Adv. Mater.* **2016**, *28*, 2601.

[208] Z. Yang, Y. Pang, X. L. Han, Y. Yang, J. Ling, M. Jian, Y. Zhang, Y. Yang, T. L. Ren, *ACS Nano* **2018**, *12*, 9134.

[209] J. Chen, H. Liu, W. Wang, N. Nabulsi, W. Zhao, J. Y. Kim, M. K. Kwon, J. H. Ryou, *Adv. Funct. Mater.* **2019**, *29*, 1903162.

[210] X. Chen, X. Li, J. Shao, N. An, H. Tian, C. Wang, T. Han, L. Wang, B. Lu, *Small* **2017**, *13*, 1604245.

[211] H. Xue, Q. Yang, D. Y. Wang, W. J. Luo, W. Q. Wang, M. S. Lin, D. L. Liang, Q. M. Luo, *Nano Energy* **2017**, *38*, 147.

[212] D. Y. Park, D. J. Joe, D. H. Kim, H. Park, J. H. Han, C. K. Jeong, H. Park, J. G. Park, B. Joung, K. J. Lee, *Adv. Mater.* **2017**, *29*, 1702308.

[213] Y. H. Joung, *Int. Neurourol. J.* **2013**, *17*, 98.

[214] X. Cheng, X. Xue, Y. Ma, M. Han, W. Zhang, Z. Xu, H. Zhang, H. Zhang, *Nano Energy* **2016**, *22*, 453.

[215] W. Han, H. He, L. Zhang, C. Dong, H. Zeng, Y. Dai, L. Xing, Y. Zhang, X. Xue, *ACS Appl. Mater. Interfaces* **2017**, *9*, 29526.

[216] W. Zhang, L. Zhang, H. Gao, W. Yang, S. Wang, L. Xing, X. Xue, *Nano-Micro Lett.* **2018**, *10*, 32.

[217] D. Ju, H. Xu, Z. Qiu, J. Guo, J. Zhang, B. Cao, *Sens. Actuators, B* **2014**, *200*, 288.

[218] Q. Zhou, W. Zeng, W. Chen, L. Xu, R. Kumar, A. Umar, *Sens. Actuators, B* **2019**, *298*, 126870.

[219] X. Xue, Y. Nie, B. He, L. Xing, Y. Zhang, Z. L. Wang, *Nanotechnology* **2013**, *24*, 225501.

[220] W. An, X. Wu, X. C. Zeng, *J. Phys. Chem. C* **2008**, *112*, 5747.

[221] Y. Fu, Y. Zhao, P. Wang, L. Xing, X. Xue, *Phys. Chem. Chem. Phys.* **2015**, *17*, 2121.

[222] Y. Nie, P. Deng, Y. Zhao, P. Wang, L. Xing, Y. Zhang, X. Xue, *Nanotechnology* **2014**, *25*, 265501.

[223] W. Zang, Y. Nie, D. Zhu, P. Deng, L. Xing, X. Xue, *J. Phys. Chem. C* **2014**, *118*, 9209.

[224] A. K S, N. P. Maria Joseph Raj, N. R. Alluri, A. Chandrasekhar, S.-J. Kim, *Sens. Actuators, B* **2020**, *320*, 128417.

**ADVANCED
SCIENCE NEWS**

www.advancedsciencenews.com

**ADVANCED
FUNCTIONAL
MATERIALS**

www.afm-journal.de

[225] M. Asadnia, A. G. Kottapalli, J. Miao, M. E. Warkiani, M. S. Triantafyllou, *J. R. Soc., Interface* **2015**, *12*, 20150322.

[226] S. Wang, J. Y. Oh, J. Xu, H. Tran, Z. Bao, *Acc. Chem. Res.* **2018**, *51*, 1033.

[227] T. Yang, D. Xie, Z. Li, H. Zhu, *Mater. Sci. Eng., R* **2017**, *115*, 1.

[228] S. Kim, Y. J. Choi, H. J. Woo, Q. Sun, S. Lee, M. S. Kang, Y. J. Song, Z. L. Wang, J. H. Cho, *Nano Energy* **2018**, *50*, 598.

[229] H. Wu, Z. Su, M. Shi, L. Miao, Y. Song, H. Chen, M. Han, H. Zhang, *Adv. Funct. Mater.* **2018**, *28*, 1704641.

[230] H. C. Liu, J. W. Zhong, C. Lee, S. W. Lee, L. W. Lin, *Appl. Phys. Rev.* **2018**, *5*, 041306.

[231] K. B. Kim, J. Y. Cho, H. Jabbar, J. H. Ahn, S. D. Hong, S. B. Woo, T. H. Sung, *Energy Convers. Manage.* **2018**, *171*, 31.

[232] P.-K. Yang, S.-A. Chou, C.-H. Hsu, R. J. Mathew, K.-H. Chiang, J.-Y. Yang, Y.-T. Chen, *Nano Energy* **2020**, *75*, 104879.

[233] W. Navaraj, R. Dahiya, *Adv. Intell. Syst.* **2019**, *1*, 1900051.

[234] Y. M. You, W. Q. Liao, D. W. Zhao, H. Y. Ye, Y. Zhang, Q. H. Zhou, X. H. Niu, J. L. Wang, P. F. Li, D. W. Fu, Z. M. Wang, S. Gao, K. L. Yang, J. M. Liu, J. Y. Li, Y. F. Yan, R. G. Xiong, *Science* **2017**, *357*, 306.

[235] M. I. Jordan, T. M. Mitchell, *Science* **2015**, *349*, 255.

[236] V. Mnih, K. Kavukcuoglu, D. Silver, A. A. Rusu, J. Veness, M. G. Bellemare, A. Graves, M. Riedmiller, A. K. Fidjeland, G. Ostrovski, S. Petersen, C. Beattie, A. Sadik, I. Antonoglou, H. King, D. Kumaran, D. Wierstra, S. Legg, D. Hassabis, *Nature* **2015**, *518*, 529.

[237] Y. H. Jung, S. K. Hong, H. S. Wang, J. H. Han, T. X. Pham, H. Park, J. Kim, S. Kang, C. D. Yoo, K. J. Lee, *Adv. Mater.* **2019**, *32*, 1904020.

[238] H. Y. Guo, X. J. Pu, J. Chen, Y. Meng, M. H. Yeh, G. L. Liu, Q. Tang, B. D. Chen, D. Liu, S. Qi, C. S. Wu, C. G. Hu, J. Wang, Z. L. Wang, *Sci. Rob.* **2018**, *3*, eaat2516.

[239] W. Li, D. Torres, R. Diaz, Z. J. Wang, C. S. Wu, C. Wang, Z. L. Wang, N. Sepulveda, *Nat. Commun.* **2017**, *8*, 9.

[240] J. Yang, J. Chen, Y. Su, Q. Jing, Z. Li, F. Yi, X. Wen, Z. Wang, Z. L. Wang, *Adv. Mater.* **2015**, *27*, 1316.

[241] S. Gong, W. Schwalb, Y. W. Wang, Y. Chen, Y. Tang, J. Si, B. Shirinzadeh, W. L. Cheng, *Nat. Commun.* **2014**, *5*, 8.

[242] J. Hirschberg, C. D. Manning, *Science* **2015**, *349*, 261.

[243] R. Fleury, D. Sounas, A. Alu, *Nat. Commun.* **2015**, *6*, 7.

[244] J. Yang, J. Chen, Y. Liu, W. Q. Yang, Y. J. Su, Z. L. Wang, *ACS Nano* **2014**, *8*, 2649.

[245] T. Yamada, Y. Hayamizu, Y. Yamamoto, Y. Yomogida, A. Izadi-Najafabadi, D. N. Futaba, K. Hata, *Nat. Nanotechnol.* **2011**, *6*, 296.

[246] J. H. Han, J. H. Kwak, D. J. Joe, S. K. Hong, H. S. Wang, J. H. Park, S. Hur, K. J. Lee, *Nano Energy* **2018**, *53*, 198.

[247] H. S. Lee, J. Chung, G. T. Hwang, C. K. Jeong, Y. Jung, J. H. Kwak, H. Kang, M. Byun, W. D. Kim, S. Hur, S. H. Oh, K. J. Lee, *Adv. Funct. Mater.* **2014**, *24*, 6914.

[248] W. Liu, J. Sun, W. Qiu, Y. Chen, Y. Huang, J. Wang, J. Yang, *Nanoscale* **2019**, *11*, 21740.

[249] W. Alquraishi, Y. Fu, W. Qiu, J. Wang, Y. Chen, L.-A. Kong, J. Sun, Y. Gao, *Org. Electron.* **2019**, *71*, 72.

[250] J. Wang, Y. Chen, L.-A. Kong, Y. Fu, Y. Gao, J. Sun, *Appl. Phys. Lett.* **2018**, *113*, 151101.

[251] J. Sun, Y. Fu, Q. Wan, *J. Phys. D: Appl. Phys.* **2018**, *51*, 314004.

[252] C. Qian, J. Sun, L.-a. Kong, Y. Fu, Y. Chen, J. Wang, S. Wang, H. Xie, H. Huang, J. Yang, Y. Gao, *ACS Photonics* **2017**, *4*, 2573.

[253] C. Qian, L.-a. Kong, J. Yang, Y. Gao, J. Sun, *Appl. Phys. Lett.* **2017**, *110*, 083302.

[254] L.-a. Kong, J. Sun, C. Qian, C. Wang, J. Yang, Y. Gao, *Org. Electron.* **2017**, *44*, 25.

[255] L.-a. Kong, J. Sun, C. Qian, Y. Fu, J. Wang, J. Yang, Y. Gao, *Org. Electron.* **2017**, *47*, 126.

[256] L.-a. Kong, J. Sun, C. Qian, G. Gou, Y. He, J. Yang, Y. Gao, *Org. Electron.* **2016**, *39*, 64.

[257] Y. He, J. Sun, C. Qian, L.-a. Kong, J. Jiang, J. Yang, H. Li, Y. Gao, *Org. Electron.* **2016**, *38*, 357.

[258] J. Yu, G. Gao, J. Huang, X. Yang, J. Han, H. Zhang, Y. Chen, C. Zhao, Q. Sun, Z. L. Wang, *Nat. Commun.* **2021**, *12*, 1581.

[259] J. Yu, X. Yang, G. Gao, Y. Xiong, Y. Wang, J. Han, Y. Chen, H. Zhang, Q. Sun, Z. L. Wang, *Sci. Adv.* **2021**, *7*, eabd9117.

[260] Y. Chen, G. Gao, J. Zhao, H. Zhang, J. Yu, X. Yang, Q. Zhang, W. Zhang, S. Xu, J. Sun, Y. Meng, Q. Sun, *Adv. Funct. Mater.* **2019**, *29*, 1900959.

[261] Q. Sun, D. H. Ho, Y. Choi, C. Pan, D. H. Kim, Z. L. Wang, J. H. Cho, *ACS Nano* **2016**, *10*, 11037.

[262] J. S. Koh, E. Yang, G. P. Jung, S. P. Jung, J. H. Son, S. I. Lee, P. G. Jablonski, R. J. Wood, H. Y. Kim, K. J. Cho, *Science* **2015**, *349*, 517.

[263] M. Wehner, R. L. Truby, D. J. Fitzgerald, B. Mosadegh, G. M. Whitesides, J. A. Lewis, R. J. Wood, *Nature* **2016**, *536*, 451.

[264] T. F. Li, G. R. Li, Y. M. Liang, T. Y. Cheng, J. Dai, X. X. Yang, B. Y. Liu, Z. D. Zeng, Z. L. Huang, Y. W. Luo, T. Xie, W. Yang, *Sci. Adv.* **2017**, *3*, 7.

[265] P. Fratzl, F. G. Barth, *Nature* **2009**, *462*, 442.

[266] M. A. Mcevoy, N. Correll, *Science* **2015**, *347*, 1261689.

[267] D. Rus, M. T. Tolley, *Nature* **2015**, *521*, 467.

[268] X. Q. Wang, C. F. Tan, K. H. Chan, X. Lu, L. L. Zhu, S. W. Kim, G. W. Ho, *Nat. Commun.* **2018**, *9*, 10.

[269] J. K. Mu, G. Wang, H. P. Yan, H. Y. Li, X. M. Wang, E. L. Gao, C. Y. Hou, A. T. C. Pham, L. J. Wu, Q. H. Zhang, Y. G. Li, Z. P. Xu, Y. Guo, E. Reichmanis, H. Z. Wang, M. F. Zhu, *Nat. Commun.* **2018**, *9*, 10.

[270] W. Q. Hu, G. Z. Lum, M. Mastrangeli, M. Sitti, *Nature* **2018**, *554*, 81.

[271] M. Sitti, *Nat. Rev. Mater.* **2018**, *3*, 74.

[272] L. Hines, K. Petersen, G. Z. Lum, M. Sitti, *Adv. Mater.* **2017**, *29*, 1603483.

[273] X. Q. Wang, K. H. Chan, Y. Cheng, T. Ding, T. Li, S. Achavananthadith, S. Ahmet, J. S. Ho, G. W. Ho, *Adv. Mater.* **2020**, *32*, 2000351.

[274] H. Lu, Y. Hong, Y. Yang, Z. Yang, Y. Shen, *Adv. Sci.* **2020**, *7*, 2000069.

[275] K. Zhang, X. Wang, Y. Yang, Z. L. Wang, *ACS Nano* **2015**, *9*, 3521.

[276] R. Cao, T. Zhou, B. Wang, Y. Yin, Z. Yuan, C. Li, Z. L. Wang, *ACS Nano* **2017**, *11*, 8370.

[277] A. Yu, M. Song, Y. Zhang, Y. Zhang, L. Chen, J. Zhai, Z. L. Wang, *Nano Res.* **2014**, *8*, 765.

[278] W. Tang, T. Jiang, F. R. Fan, A. F. Yu, C. Zhang, X. Cao, Z. L. Wang, *Adv. Funct. Mater.* **2015**, *25*, 3718.

[279] Z. Wen, J. Chen, M.-H. Yeh, H. Guo, Z. Li, X. Fan, T. Zhang, L. Zhu, Z. L. Wang, *Nano Energy* **2015**, *16*, 38.

[280] S. Ornes, *Proc. Natl. Acad. Sci. USA* **2016**, *113*, 11059.

Xiaole Cao received his B.E. degree from Tianjin University of Science and Technology in 2019. Now he is a master candidate in Beijing Institute of Nanoenergy and Nanosystems, Chinese Academy of Sciences. His research interests include energy harvesting, self-powered sensors, and intelligent application based on triboelectric nanogenerator.

Yao Xiong received her bachelor's degree from University of Science and Technology Bejing in 2019. Now she is a master candidate in Beijing Institute of Nanoenergy and Nanosystems, Chinese Academy of Sciences. Her research direction mainly includes energy harvesting, self-powered sensors and corresponding intelligent application.

Xiaoxiao Zhu received her Ph.D. from Bunka Gakuen University in 2017. Then, she worked as research assistant in Culture and Environmental Clothing Studies Research Institute. She has joined in Beijing Institute of Fashion Technology as a professor since 2018. Her main research interests include clothing ergonomics, environmental clothing studies, somatometry, 3D motion capture, thermal manikin applications for garments comfort, wearable energy-harvesting strategy, etc.
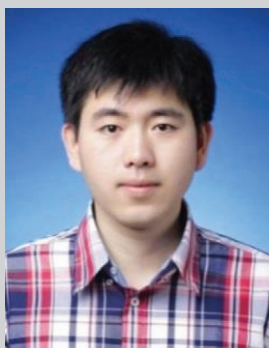
Qijun Sun received his Ph.D. from Gachon University in 2013. After that, he worked as a postdoctoral researcher in POSTECH and SKKU until 2015. From 2016, he has joined Beijing Institute of Nanoenergy and Nanosystems, CAS, as the principal investigator of Functional Soft Electronics Lab. The main research interests of his group include triboiontronic devices, mechanoplastic neuromorphic transistors, artificial synaptic devices electronic skin, 2D materials based flexible semiconductor devices, human-machine interactive systems and micro-nano fabrication, aiming to develop advanced systems for human health monitoring and human-robotic interface.

**ADVANCED
SCIENCE NEWS**

www.advancedsciencenews.com

**ADVANCED
FUNCTIONAL
MATERIALS**

www.afm-journal.de

Zhong Lin Wang received his Ph.D. from Arizona State University in physics. He now is the Hightower Chair in Materials Science and Engineering, Regents' Professor, Engineering Distinguished Professor and Director, Center for Nanostructure Characterization, at Georgia Tech. Dr. Wang has made original and innovative contributions to the synthesis, discovery, characterization and understanding of fundamental physical properties of oxide nanobelts and nanowires, as well as applications of nanowires in energy sciences, electronics, optoelectronics and biological science. He pioneered the field of piezotronics and piezo-phototronics by introducing piezoelectric potential gated charge transport process in fabricating new electronic and optoelectronic devices.